ATOMIC PHYSICS AND THE POLAR CAP*

A. E. S. Green and D. J. Strickland

Department of Physics and Astronomy

University of Florida, Gainesville 32601

*Supported in part by National Aeronautics and Space Administration Grant ~~NsG-599~~ NGL-10-005-008

1. INTRODUCTION

One might organize a discussion of fundamental mechanisms in polar cap phenomena in the light of the special morphological features of these phenomena as distinct from auroral zone or other upper atmospheric phenomena. Alternatively, one might approach the topic from the standpoint of atomic physics, a fundamental discipline intimately entwined with all aeronomical phenomena. Here we begin with a section which describes the characteristics which distinguish the polar cap region from the auroral zone and lower latitude regions. Then we essentially adopt the latter approach and, in this context, will concentrate on three important types of processes:

A. processes stimulated by photons

B. processes stimulated by electrons

C. processes stimulated by protons.

In photon induced processes, the longer slant paths followed by the energetic solar photons over the polar cap leads to energy deposition at higher altitudes. In electron and proton induced processes, there are differences in the geomagnetic field configuration and in the character of the incident fluxes. The mirroring particles in the polar cap region do not follow 'trapped' particle trajectories, but instead become lost in the tail region of the geomagnetic field. However, our

interest here is primarily in those particles which interact and thereby lose their energy to the atmosphere. In terms of atomic processes, we thus look for unique features of the polar cap region, particularly auroral phenomena through the character of the incident changed particle fluxes.

In Section 3, 4, and 5, we will review the broader outlines of general aeronomical processes stimulated by photons, electrons, and protons, respectively. We will where possible concentrate on aspects of these processes which require special emphasis in polar cap phenomena. With this approach, this work might also serve as a general review of the state of knowledge of atomic physics and planetary aeronomy. This relationship is so intimate and demanding that, undoubtedly, both fields must go forward together.

2. Particle Morphology in the Polar Cap

As noted in the introduction, the distinguishing feature of the polar cap from the viewpoint of atomic processes is the character of the incident particle fluxes. To orient ourselves, we first give here a brief morphological description of electron and proton fluxes and accompanying auroras as observed in the cap region.

In the description to follow, it will be helpful, for the sake of orientation, to define the boundary of the cap region. One can loosely define this as the high latitude boundary of the auroral oval. The oval and polar cap region are shown in Fig. 1 in terms of the standard coordinates of local magnetic time and invariant latitude.

The polar cap region is particularly responsive to solar activity. This is due to the connection of its magnetic field lines to the magnetotail and to the solar wind. In addition flare-produced X-rays (sudden ionospheric disturbances) have an interesting aspect because such X-rays impinge upon the upper regions of the polar cap near grazing incidence.

We also frequently encounter very low energy electron stimulated phenomena and often at very high altitude. Furthermore, protons play a more important role in the polar cap region than in the auroral region.

A detailed picture of particle precipitation and its consequence in the cap region has not yet been formulated. There have been, however, sufficient satellite and ground observations over the last decade to indicate the major controlling elements in polar cap phenomena and to catalogue the various types of particle fluxes and their atmospheric consequences.

(a) The Solar Wind and Magnetotail

The solar wind [Mackin and Neugebauer (1)] flowing outward from the sun stretches the earth's magnetic field lines, particularly those connected to the polar cap into an extended magnetotail. A neutral sheet develops in a region of field reversal between the northern and southern halves of the magnetotail [Ness (2)]. This neutral sheet is embedded in a region of plasma which has an enhanced energy necessary to prevent the collapse of the field

[Axford et al (3)]. Extensive data relative to the magnetotail has been observed from Vela and OV3 satellites [Bame et al, (4) , and Montgomery et al, (5)].

The role of the plasma sheet in the magnetotail in relation to the diversity of phenomena encountered in the auroral and polar cap regions is still uncertain. This plasma sheet, according to Hones et al (6), is a region containing electrons and protons at a density of 0.1p/cc to 1 p/cc. Frequently, energetic electrons with energies greater than 45 keV are observed. At large L values, the plasma sheet extends from the dawn to dusk boundary of the magnetotail and is often quite thick. This plasma sheet apparently flaps up and down around the Earth's axis in response to the motion of the Earth's magnetic axis.

The particular features of the polar zone which influence greatly the characteristics of the stimulating charge particles are the large L values of the earth's magnetic field. By virtue of this, the charged particles are linked to the very far outer regions of the

magnetosphere and also possibly to the sun. Thus, energetic electrons of solar origin have uniform access to the polar caps and the fluxes are essentially independent of the altitude over wide ranges. Furthermore, polar cap energetic electrons are always found to be accompanied by energetic protons. Hones et al.(7) also studied the relationships of electrons at high altitudes over the auroral and polar region and those at 17 Earth radii in the plasma sheet of the magnetotail. They have shown a significant correlation between its two regions. In addition, they have noted that auroral zone x-rays correlated strongly with observations on Vela satellites. For example, they noted on six occasions, a detection of bursts of energetic electrons which were clearly related to x-ray bursts observed by balloon borne instruments.

The detailed plasma mechanisms and magnetospheric phenomena which explain the observations of particles in the polar cap are quite complex. We refer the reader to the recent reviews of Bame (4), Hones (6) and recent conference proceedings McCormac and Omholt (8) and the articles in this issue by Reid (9) and Hakura (10) for a more detailed guide to the literature.

(b) Particles

We list the following fluxes without regard, in general, to their correlation with such geophysical parameter as phase of the solar cycle, season, universal and local time, and magnetic activity:

(1) soft electron fluxes ($\lesssim$ a few kev) between $\sim 73^{\circ}$ and 82° invarient latitude [see Johnson and Sharp (11), Burch (12), Hoffman and Evans (13), Hoffman (14), and Maehlum (15)]

(2) hard electron spikes (>40 kev) on the nightside [see McDiarmid and Burrows (16) and McCoy (17)]

(3) electron fluxes characteristic of those producing active evening oval auroras and associated with severe global magnetic storms

(4) proton and α particle fluxes generated by solar

flares and associated with PCA [see, e.g., O'Brien (18)]

(5) electron fluxes generated by solar flares [Vampola (19)].

Items (3) and (5) have relatively rare occurances and may be listed as special events. To our knowledge, the electron fluxes in (3) have not been observed but can be predicted from those rare active auroras which have been observed during great global magnetic storms [Lassen (20)]. The auroras behave similar to the active auroras in the evening sector of the oval and in fact are probably associated with the oval which is known to expand during the onset of magnetic storms [Akasofu (21)].

The proton and α particles in (4) are highly energetic (typically > 1 Mev) and their fluxes dissipate considerable energy in producing PCA and polar glow aurora [Sandford (22)]. Blake et al. (23) have observed solar protons in the energy range from 1.1 to 1.6 Mev and alpha particles in the energy range from 4.1 to 15 Mev over the polar caps associated with the proton event of August 28, 1966. A persistant and ordered latitudinal structure suggested an effect associated with non-uniform access of solar protons to high latitudes. They observed pitch-angle distributions that delineated a region of quasi-trapping. They found no evidence for a durable containment of quasi-trapped solar alpha particles.

Paulikus et al.(24), have observed solar protons in the 1 to 100 Mev interval during a solar proton event of September 2, 1966. They found an important day-night asymmetry

in the geo-magnetic cut-off and the flux started to decrease from the polar plateau value at higher invarient latitudes nearer the noon meridian than the midnight meridian. The asymmetry was more pronounced for low energy particles. The pitch-angle distribution suggested that a quasi-trapped flux of protons is established at high latitudes on the day side of the polar cap. They found a limited access of solar protons to some local times and that this was associated with mid-day absorptions recoveries observed with riometers.

Of considerably less importance during PCA events are the electron fluxes in (5). Although very energetic ($\gtrsim$ 100 Kev), they comprise a small fraction of the energy of the total particle flux and are often not observed to accompany the protons and heavier ions [Vampola (19)].

The soft electrons in (1) refer to flux above the aurora zone and above, say, the 40 kev cutoff boundary which exhibits a strong enhancement below a few kev compared to adjacent flux in the aurora zone. The soft flux exhibits a zonal pattern between about 73^0 and 82^o and as a result this region has become known as the soft zone. Based on Burch's (12) observations, this pattern appears to be a permanent feature. Above 85^o, there appears to be a general lack of the flux except during special events. Although the soft flux is distinctive at high latitude, the energy content is rather low. Below 5 kev where much of the energy is contained [Burch (12)] one can expect values $<<$ 1 erg/cm^2-sec-ster. There is, however, very sporatic behavior to the flux such that energies well above 1 erg/cm^2-sec-ster can be observed as spike type events.

C. Auroras

Based upon visual, photographic, and photometric observations we list the following auroras occurring over the polar cap:

(1) Discrete morning auroras [see e.g. Lassen (25) and Sandford (26)]

(2) polar cap auroras [Davis (27)]

(3) active auroras accompanying global magnetic storms [Lassen (20)]

(4) polar glow auroras [Sandford (28)].

The list excludes the auroras occurring in the aurora zone, namely the discrete nighttime auroras [Sandford (26)], i.e. the traditional active aurora, and also the mantle aurora [Sandford (26) and Hartz and Bryce (29)]. Both types are found below the cutoff boundary and are thus of no interest in the present study. We define the mantle aurora as the emission produced by those hard, steady electron fluxes (> 20 kev) having a strong morning maximum but occurring below the cutoff boundary. Sandford defines the mantle aurora as that glow in the absence of observed discrete auroras. Based on his observations [Sandford (26)] the mantle aurora extends, at times, to latitudes well above the cutoff boundary and would then not correspond to the above definition. As Eather and Akasofu (30) point out, however, Sandford was probably observing, in addition to the mantle aurora as defined above, subvisual, patchy auroras

above the cutoff boundary believed to be caused by the soft zone fluxes.

Because the previously listed fluxes are responsible, at least in part, for the auroras (1) - (4) above, it is natural to follow a similar classification, namely, into special and ordinary events. Included under special events are (3) and (4) which correspond to fluxes (3) - (5). The active auroras in (3) commence at the onset of great magnetic storms and may be seen overhead even at the magnetic poles. The polar glow aurora (4) is a diffuse glow covering the whole polar cap and results from proton precipitation following a solar flare event. Also accompanying the glow is PCA. As mentioned, energetic electron fluxes which may accompany the proton and α particle fluxes do not contribute significantly to the total energy input [Vampola (19)].

Included among the more ordinary auroras are (1) and (2). The discrete morning auroras are approximately situated in the soft zone and have a distinct late morning peak. Lassen (20) has also observed a weaker afternoon peak for the same type of aurora. As described by Lassen (25), the morning auroras are in the form of faint diffuse bands or draperies of long quiet rays and all have a general quiet appearance. In addition, Eather and Akasofu's (30) observations indicate that auroras having a more patchy appearance also occur in and near the morning soft zone. The morning auroras are not thought to be associated with

the morning sector of the oval even though the high latitude boundary does approach 80°. The oval auroras are observed to approach, but do not seem to mix with the discrete morning auroras, at least during the quiet times [Lassen (25)].

The source of the morning auroras is most likely the soft fluxes of the soft zone [Eather (31) and Eather and Akasofu (30)]. This is a natural assumption to make although available soft flux data does not show an obvious late morning enhancement. In support of the soft flux source, however, are measurements by Starkov (32) which show the lower altitude boundaries of the morning auroras to be near 150 km. This is not confirmed, in general, however, by Lassen (25) although his observations do show that morning auroras are situated at higher altitudes than the discrete nighttime auroras.

Based on, e.g. Burch's (12) soft flux measurements, typical intensities of the 3914 A band will be well below 100 R. Eather and Akasofu's (30) photometric measurements of morning auroras confirm that the intensity is generally low, in fact lower than typical values predicted from the soft flux data. From the observed character of the soft fluxes, however, a wide range of intensities can be expected although subvisual auroras are probably the rule rather than the exception.

To complete our list of auroras, the polar cap auroras (2) [Davis (27)] have the same general quiet appearance of the morning auroras but are located above 80°.

whereas morning aurora with band structure lie in a general direction parallel to the oval boundary, the cap aurora are aligned in the direction of the sun; i.e. in a north-south direction. Davis (27) observes a distinct anti-correlation with magnetic activity. Although less obvious, there are indications that morning auroras also exhibit anti-correlation [Sandford (26)]. Based on similarity in appearance and possible common anti-correlation, the flux characteristic of the polar cap and morning auroras may be very similar. Soft fluxes may then also provide most of the energy producing polar cap auroras.

In presenting the above lists of fluxes and auroras, we have not attempted to fit them into a general picture. To do so would require consideration of the various geophysical parameters such as phase at the solar cycle, universal and local magnetic time and magnetic activity. A good example of efforts along this line is given by Sandford (26) who has established certain statistical relationships between auroras and some of the parameters listed above. Our purpose has rather been with the idea of identifying as many distinct events as have presently been observed and, in particular, to note the relative importance of soft precipitating fluxes above the cutoff boundary.

Perhaps we should mention that the hard electron spikes (2) observed by McDiarmid and Burrows (16) will have associated with their spike type auroras which are probably considerably more intense than the soft flux auroras. Based on the flux data, however, they occur with considerably less frequency.

One type of flux missing from our list is a more or less "steady" flux which in turn would produce a diffuse glow.

During January and February, 1968, Eather (31) observes no measurable steady glow which could be attributed to such a source. In addition, available flux data does not show any steady source which could produce a measurable glow. Sandford's (26) data, however, would seem to suggest a steady glow having maximum intensity near solar maximum. As suggested by Eather and Akasofu (30), however, this apparent glow may arise from subvisual "morning" type auroras.

3. PROCESSES STIMULATED BY PHOTONS

(a) Overview

Photons are particle manifestations of the electromagnetic field and, because of our vast background in classical and quantum electrodynamics, photon induced processes should, in principal, be well understood. The photon interaction processes of primary interest are (1) total absorption, (2) Rayleigh scattering, (3) resonance scattering, (4) flourescence, and (5) photoelectron production. We will give primary attention to the photoelectron produced dayglow because of a specific background of recent effort related to this topic [see, e.g., Hinteregger et al(33), Green and Barth (34), and Dalgarno et al. (35)].

In Figure 2 we show, in block diagram form, the steps involved in calculating the dayglow spectral line intensities stimulated by the extreme ultraviolet and X-ray radiations (10eV to 1kev) of the sun. The figure illustrates the many facets of atomic physics and atmospheric physics which play a part in the interpretation of spectral observations, not only from the ground, but also from rockets and satellites.

The categories 1 and 2 represent the information needed to arrive at the extreme ultraviolet (XUV) flux incident at the upper boundary of earth's atmosphere.

The next two items are needed to arrive at the local intensities of XUV at any altitude in the atmosphere. In step 5 the conversion of XUV photons to electrons proceeds primarily via the photoelectric and Auger effects. To describe the production rates, we must know the fundamental σ_{ph} and σ_{au} cross sections of the atmospheric species in the range of photon energies of importance. Such photon cross sections are still rather uncertain atomic parameters and precise experimental data in this region has only recently become available [see, e.g., Cook and Metzger (36), Frost et. al. (37), and Schoen (38)]. With the aid of these recent data, it is now possible to arrive at the local electron spectral density resulting from photon primaries from the sun.

Starting with step 6 we must next concern ourselves with the details of all excitation, ionization, and other processes which are induced locally by these photoelectrons at the various altitudes. We will address ourselves to detailed features of electron energy deposition in the next section, but will first consider some of the general features. At this point, the aeronomical problem becomes very difficult and unconventional with respect to typical problems in pure atomic physics. This is due to the necessity of knowing all inelastic cross sections and not just the specific cross sections related to states which emit the spectral lines of interest. With these cross sections, we construct the loss function or stopping power, which is

a key entity in the analysis of the energy balance. For a single species this is defined as a function of the electron energy E given by:

$$\frac{1}{n}\frac{dE}{dx} = L(E) = \Sigma_j \sigma_j(E)W_j + \Sigma_i I_i \sigma_i(E) + \Sigma_i \int_0^{(E-I_i)/2} S_i(E,E_s)\, E_s dE_s + \Sigma E_d \sigma_d(E) \qquad (3.1)$$

The successive terms represent the loss contributions due to excitation of atomic or molecular states with excitation energies W_j, ionizations with threshold energies I_i which produce a continuum of secondary electrons E_s, dissociations with threshold energies E_d, and other significant processes. The symbols $\sigma_j(E)$, $\sigma_i(E)$, $S(E, Es)$ and $\sigma_d(E)$ denote the cross sections for the corresponding processes and n denotes the number density of the given species.

The atomic-aeronomical problem is further complicated by the fact that atmospheric mixtures of gases have altitude dependent concentrations. Then the total loss function also depends upon altitude y . It may be calculated using:

$$L(E,y) = \Sigma_\ell \phi_\ell (y)\, L_\ell (E) \qquad (3.2)$$

where ℓ denotes the ℓth species,

$$\varphi_\ell(y) = n_\ell(y)/n(y) \text{ and } n = \Sigma_\ell n_\ell$$

If all of the atomic and aeronomical quantities referred to in Eq.'s 3.1 and 3.2 are known, it possible (step 8) to calculate the total energy deposited in the j^{th} state of the ℓ^{th} constituent for any photoelectron with energy E_p using the continuous slowing down approximation:

$$E_{j\ell}\ (E_p,y) = \phi_\ell\ (y) \int_{W_j}^{E_p} \frac{W_j\ \sigma_j\ (E)}{L(E,y)}\, dE \qquad (3.3)$$

We assume local loss at altitude y although as already noted L(E,y) is constructed such that as we move from one altitude to the next, the proper altitude dependence is taken into account.

The next step (9) is to determine the secondary electron spectrum associated with the slowdown of each photoelectron. Here, if the differential cross sections for each ionization continuum are known, it is possible to generate the secondary electron spectrum in the degradation of the primary electron to zero energy using:

$$n_{i\ell}\ (E_p,E_s,y) = \phi_\ell\ (y) \int_{2E_s + I_i}^{E_p} \frac{S_{i\ell}\ (E,Es)}{L(E,y)}\, dE \qquad (3.4)$$

This process must be carried out for each component of the photoelectron spectrum to arrive at a net secondary electron spectrum. Once the complete secondary electron spectrum is known, the problem

becomes that of calculating the energy transferred to the j^{th} state via every component of this spectrum. This can be done by straightforward reiteration of the techniques used to treat the original photoelectron spectrum. Thus, one can go through the process again to arrive at the tertiary spectra. This is then divided into many elements and their contributions to the population of the j^{th} state determined. Fortunately, this approach converges rapidly and usually the fourth generation is relatively insignificant. It is also possible to solve for the complete population increase of the j^{th} state by use of an integral equation [Peterson and Green, (39)].

One must next consider cascading which can indirectly populate lower states and consequently produce two or more emission frequencies from a given higher state. For such calculations one must know the entire array of transition probabilities associated with the atmospheric atom and molecules. In the case of molecular emissions, the entire electronic band system strength may be subdivided into band oscillator strengths through the use of Franck-Condon factors [Barth, (40)].

At this point (12) one must give particular attention to metastable states which play an important role in upper atmospheric phenomena. When the radiative lifetime of such states is comparable to the mean time between collisions, collisional deactivation must be considered. The process often has a large influence, particularly at the lower altitudes.

Certain states are also significantly populated by chemical reactions. In the case of OI ^1S excitation, e.g., dissociation recombination by O_2 rather than direct electron impact on OI is known to be the dominant excitation process [Donahue et al.(41)]. Thus, we must have a knowledge of reaction rate coefficients to properly treat the entire problem.

We next must concern ourselves with the transfer of radiation from the source to the detector. If the atmosphere is thin with respect to a line of interest we need simply allow for attenuation losses. This brings us back to consideration of Chapman function already mentioned with respect to Step 2. We will treat this more fully in 3b. If we are, however, dealing with a resonance line in which the atmosphere is optically thick then a more complete radiative transfer calculation is needed.
Such a calculation will be described in 3c.

We see, finally, that the first 13 steps illustrated in Fig. 1 lead to a theoretical result which can then presumably be compared with experiment. Agreement presumably means we understand the problem and we have given the correct inputs. Disagreement, however, forces us to reassess either the assumed aeronomical properties or the assumed atomic properties. Our experience has indicated that the chance that we must change the aeronomy or the atomic physics are approximately the same at this point of time. Thus, from the viewpoint of input quantities needed in dayglow calculations, we find that atomic physics is approximately at the same undeveloped level as is atmospheric physics.

b Generalized Chapman Function

In connection with his theory of the formation of the ionosphere, Chapman[42] considered the absorption of the sun's radiation near grazing incidence by the earth's atmosphere. The same attenuation problem arises more critically in the polar cap region even during the daylight hours.

Figure 3 illustrates the geometry of the problem. Here we use the coordinates y_0 to denote the altitude of the observer, and θ_0 to denote the zenith angle. A slant path CS is drawn to the sun (we ignore refraction) and a general element, ds, along this slant path is positioned by y and the angle θ_y relative to the line joining the source to the center of the earth. From geometry it follows immediately that

$$\frac{\sin \theta_y}{R + y_0} = \frac{\sin \theta_0}{R + y} \tag{3.5}$$

Solving for sec θ_y, we find

$$\sec \theta_y = \left[1 - \left(\frac{R+y_0}{R+y}\right)^2 \sin^2 \theta_0\right]^{-1} \tag{3.6}$$

In an absorbing medium, the reduction in intensity in an element of slant path ds at an altitude y is given by

$$dI/I = -\sigma n(y)ds = -\sigma n(y)dy \sec \theta_y \tag{3.7}$$

where σ, the absorption cross section for the particular atmospheric species, is assumed to be independent of altitude. We next integrate Eq.3.7 along a slant path and along a vertical path to establish the transmission $e^{-\tau}$ and $e^{-\tau_v}$ where τ and τ_v are the optical depths along the slant path and vertical path respectively.

The generalized Chapman function may then be defined as

$$gch(\theta, y_0) = \frac{\tau}{\tau_v} = \frac{\int_{y_0}^{\infty} n(y) f(\theta, y_0, y) dy}{N(y_0)}, \tag{3.8}$$

where $f(\theta, y_0, y) = \sec(\theta_y)$

and

$$N(y_0) = \int_{y_0}^{\infty} n(y)dy \tag{3.9}$$

is the column density

Chapman considered the case in which n(y) follows as a simple exponential law. Tables for this case have been developed by Wilkes (43).

The more general case in which n(y) corresponds to any distribution function has been considered by Green and Martin(44). We consider here a simplification of their treatment.

We may choose y, θ_y, or ϕ, the angle shown in the figure, as the independent variable of integration; however, a more convenient variable of integration is

$$u = (y - y_0)/(R + \gamma_0) \tag{3.10}$$

Then $\sec \theta_y$, which we shall henceforth refer to as f(u), may be placed in various forms.

$$f(u) = \sec \theta_y = \left[1 - \frac{\sin^2 \theta}{(1 + u)^2}\right]^{-\frac{1}{2}} \tag{3.11}$$

$$= \frac{1 + u}{(\gamma^2 + 2u + u^2)^{\frac{1}{2}}}, \qquad \gamma = \cos \theta \tag{3.12}$$

or

$$f(u) = f_e(u) + f_r(u) \tag{3.13}$$

where

$$f_e(u) = (\gamma^2 + 2u)^{-\frac{1}{2}} = \sec \theta [1 + (2u/\gamma^2)]^{-\frac{1}{2}} \tag{3.14}$$

and

$$f_r(u) = \left[\frac{1 + u}{[1 + u^2 f_e^2]^{\frac{1}{2}}} - 1\right] f_e(u) \tag{3.15}$$

The function $f_e(u)$ has the essential features of f(u) everywhere, including near $\theta = 90°$ where it becomes singular as $u^{-\frac{1}{2}}$ near $u = 0$. The function $f_r(u)$ is well behaved and small everywhere.

We now turn our attention to $f_e(u)$, the essential part of $f(u)$. Using equation 3.14 we have as the essential part of our generalized Chapman function

$$gch_e(\theta,x) = \int_0^\infty \frac{n(u)\ du}{(\gamma^2 + 2u)^{1/2}} = \sec\theta \int_0^\infty \frac{n(u)}{(1 + 2u/\gamma)^2}\, du \qquad (3.16)$$

For most distribution functions it is not possible to evaluate this integral analytically. However, the integrand usually will have the essential properties of the exponential distribution for large values of the independent variable. Accordingly, it is convenient everywhere except (i.e., $\theta \sim 90°$) to evaluate $gch_e(\theta, x)$ with a Laguerre integration procedure using a limited number of points [see a handbook of mathematical functions].

In the immediate neighborhood of $\theta = 90^\circ$ or $\gamma = 0$ the singularity at the origin presents a problem. We may resolve this problem, however, by transforming to the variable

$$z = \left(2u + \gamma^2\right)^{1/2} - \gamma \qquad (3.17)$$

Then equation 3.16 becomes

$$gch_e(\theta,x) = \int_0^\infty n\left[\frac{(z+\gamma)^2 - \gamma^2}{2}\right] dz. \qquad (3.18)$$

This integral may now be evaluated with the same Laguerre integration technique. This technique works particularly well as long as γ is not too large. Thus Equation 3.16 and Equation 3.18 complement each other, the latter being useful from 90° to say 60° the former from 0° to say 80°. The residual part of f(t) is small and smooth everywhere so that its contribution can be estimated in a variety of ways. The simplest is to replace $f_r(u)$ by $f_r(\bar{u})$ where $\bar{u}$ is the average with respect to n(u). A Laguerre integration scheme should give results to any desired precision.

We should note that if the 90° case can be dealt with, we can also treat angles greater than 90°. In Figure 3 we illustrate a case in which θ_0 is greater than 90°. It should be obvious from the diagram that the equivalent thickness for the slant path AB is

$$\tau_{AB} = 2\tau_{BE} - \tau_{AD}. \tag{3.19}$$

Since each optical depth is given by

$$\tau = \int_{y}^{\infty} n(y) f(\theta, x, y)\, dy. \tag{3.20}$$

it follows that

$$\int_{y_o}^{\infty} n(y) f(\theta,x,y)\,dy = 2\int_{y_b}^{\infty} n(y) f(\tfrac{\pi}{2},b,y)\,dy - \int_{y_o}^{\infty} n(y) f(\pi - \theta,x,y)\,dy. \tag{3.21}$$

And hence

$$gch(\theta,x) = 2\,\frac{N(y_b)}{N(y_o)}\,gch\,(\tfrac{\pi}{2},\ x \sin\theta) - gch(\pi - \theta,x), \tag{3.22}$$

where we have used the relation

$$x_b = x \sin\theta_o = x \sin\theta. \tag{3.23}$$

3(c) Radiative Transfer

In arriving at step 13 in fig. 2, we have the altitude dependent volume production rate via principally electron impact. We must then take account of imprisonment of radiation for those lines affected by this mechanism. Here, we limit our discussion to atomic lines. To know whether imprisonment, or in other words, multiple scattering, is important, we need only consider the total line center optical depth of a given line, designated by τ. The line center optical depth at altitude z is given by

$$\tau(z) = \sigma_0 \int_z^\infty n(z')dz' \tag{3.24}$$

where $n(z)$ is the density of the corresponding species and σ_0 is the resonance cross section at line center (i.e. at $\nu = \nu_0$ where ν_0 is the center resonant frequency). Designating z_0 as the effective lower boundary of the medium, the total effective depth τ_0 then refers to this altitude. For those lines for which τ_0 is less than unity, there is a high probability that a photon will escape the medium without a resonance absorption and, consequently, imprisonment will not be effective. Some of the important atomic lines to which this applies are OI 6300 A, OI 5577 A, and OI 1356 A.

There are many other lines, however, for which τ_0 is large enough that the probability of direct escape from the point of emission is small. Some of the important lines to which this refers are OI 1304 A, NI 1200 A, HI Lα (1216 A) HI Lβ (1027 A), and HeI 584 A. To such lines, the methods of radiative transfer must be applied. We refer the reader to such papers as [Thomas (46)], [Donahue (47)], and Strickland and Donahue (48).

Basically, we are faced with the problem for which the total volume emission rate is not equal to that produced by the initial excitation source (such sources are photoelectrons and solar resonance photons in the dayglow and precipitating electrons in electron auroras). The total rate is necessarily greater with the difference resulting from the imprisoned photons. The greater the total depth τ_0 the greater will be this imprisonment and in turn the greater the total volume emission rate relative to that produced directly by the initial source. We designate the emission rate produced by the initial source by $S_0(z)$ and the total rate by $S(z)$. Each has the units photons emitted/cm^3-sec with the photons distributed over an appropriate normalized frequency profile (for details as to how line frequency is treated, see the above mentioned references regarding radiative transfer).

In a problem of the nature we are discussing, in arriving at step 13, we have determined the function $S_0(z)$. For the boundary conditions given by the properties of the medium, for the given $S_0(z)$ and with a knowledge of how to properly treat the frequency dependence, we arrive at a unique total volume emission rate $S(z)$ via the transport equation. It is then a simple matter to derive the intensity from

$$4\pi I(z,\mu) = \int_z^\infty S(z)\ T[(z'-z)/\mu]\ dz'/\mu \qquad (3.25)$$

where $4\pi I$ is the intensity (in photons/cm^2-sec-4πster), T is the "transmission" function which gives the probability that a photon will travel the distance $(z'-z)/\mu$ without an absorption and μ is the cosine of the zenith angle, which, for the given integration limits, assumes values between 0 and 1 (again, for details concerning Eq. 3.25 as well as the transport equation, see the above-mentioned references).

For those lines unaffected by transport effects, Eq. 3.25 reduces to

$$4\pi I(z,\mu) = \int_z^\infty S_0(z')dz'/\mu\ . \qquad (3.26)$$

We thus note that, as transport effects become less important, the function $T[(z'-z)/\mu]$ approaches unity and total rate $S(z)$ approaches the initial rate $S_0(z)$.

4. PROCESSES STIMULATED BY ELECTRONS

4(a) Analytical Approach

In this section we consider the calculation of spectral emissions stimulated directly by electrons incident upon the upper atmosphere (see Figure 4). Of course the incident spectral flux must be specified (item 1). Here the geometric problem is greatly complicated by the controlling influence of the geomagnetic field (item 2). Again, the altitude distributions of the atmospheric species play an important part (item 3).

We must next be able to deal with the spatial aspects of the energy deposition of the primary electrons which, from first principles, is a highly complex problem. Multiple scattering, straggling, and other difficult aspects of charge particle degradation enter in an essential way. Work to date on the geometric aspects of primary penetration has largely been dealt with by scaling [see, e.g. Rees (49) and Stolarski (50)]. In principle, it should be possible, using Monte Carlo techniques, to deal with this problem fundamentally if all electron impact cross sections for scattering, excitation, ionization, and other processes were known (item 4). With such

information, one could chart the course of individual electrons penetrating into the atmosphere guided by the magnetic field lines and redirected in their path by encounters with the gaseous atoms and molecules. At this time, such an ambitious project has not been undertaken by the Florida group, but rather a more local approach has been used which allows us to pick up the procedure at step 6 in Fig. 2.

Referring back to the previous section, we saw from step (6) onward the major role which electron impact cross sections play in the calculation of the emissions. Progress until recently has been greatly retarded by the lack of knowledge of such cross sections. However, in a series of studies initiated in 1963, [Green et al. (51)] a technique of semi-empirical cross sections (SECS) has been used to provide approximate cross sections for all excitation and ionization processes which play a role. Essentially, the method is based upon the Born-Bethe concept of generalized oscillator strengths. To allow for the breakdown of the Born-Bethe approximation at low energies, empirical modification factors are incorporated into the generalized oscillator strengths whose

magnitudes and shapes are guided by experimental observation of differential cross sections. The power of the method rests largely on the fact that generalized oscillator strengths go over to the corresponding optical oscillator strengths (proportional to photon cross sections) in the limit of zero momentum transfer. This connection with photon impact cross sections is helpful in many cases to establish the overall magnitude of electron impact cross sections. This constitutes the major advantage of this systematic approach based upon wave mechanics with respect to an alternative systematic technique due to Gryzinski[52], which is based upon classical mechanics.

Essentially, one may view the modified generalized oscillator strengths as a scaling procedure in which one assumes that all the generalized oscillator strengths associated with a Rydberg series of transitions conform to a scaling law:

$$\sigma(n,W,x) = (n - \delta)^3 W_n^{-2} F(z) \qquad (4.1)$$

where n is the principal quantum number of the Rydberg series, δ is the corresponding quantum defect, W_n is the energy loss, $F(z)$ is a universal function, and $z = x/(W_n/R_e)$ where x and R_e are respectively the square of the momentum transfer and the Rydberg energy.

The specific methods of utilizing the generalized oscillator strengths involve a choice of certain parameterized analytic forms for F(z) which can be readily integrated over all angles of scattering to arrive at the total discrete and differential ionization cross sections. A subsequent integration of the differential cross section (usually numerical) over the range of ejected electron energy gives us the total ionization cross. The determination of parameters is based on available generalized and optical oscillator strength data, direct impact cross section data, systematics which arise among similar types of states, systematics among the gases themselves and quantum mechanical considerations.

The derived cross sections are then replaced by analytic forms chosen to facilitate execution of the degradation calculations. In recent calculations, the forms used have been:

$$\sigma_j(E) = \frac{q_o f_o c_o}{W_j^2} \left(\frac{W_j}{E}\right)^{\Omega} \sum_{s=o}^{n} a_s \left(\frac{W_j}{E}\right)^{\Gamma s} \tag{4.2}$$

and

$$\frac{d\sigma_i(E,W)}{dW} = \frac{q_o A_o}{W^2} \left(\frac{I_i}{E}\right)^{p} \left(\frac{W}{E}\right)^{\Omega} \sum_{s=o}^{n} a_s \left(\frac{W}{E}\right)^{\Gamma s} \tag{4.3}$$

where W_j and I_i refer respectively to the j^{th} discrete and i^{th} ion state. The constant $q_o = \pi a_o^2 (2R_e)^2 = 6.51 \times 10^{-14}$ cm^2 ev^2, $F_o c_o$ and A_o are magnitude parameters and the a's are restricted by $\sum a_s = 0$ which forces the cross sections to zero at threshold as required. At most, three terms in the sum are needed to achieve acceptable fits to the semi-empirical forms or to direct data where available.

In our degradation calculations one of the key problems is the calculation of the secondary electron spectrum associated with the degradation of a primary particle (Eq. 3.4) previous section). Here the problem becomes one of calculational design, and one can become easily bogged down in matters involving the second digit when the first digit is still the point in question. It is at this point that a simplification in the overall calculations can be accomplished if one can represent loss functions, determined from microscopic calculations such as given by Eq. 3.1 by a simple analytic form.

The feasibility of such a technique has been established by Green and Stolarski (53) who proposed the loss function in terms of an equation:

$$L(E) = L_o \left[\Sigma (E/E_j)^{\Omega_j}\right]^{-1} \qquad (4.4)$$

where the coefficients for any substance can be established, using certain rules [Green and Peterson (54)].

For this form of the loss function, Eq (4.3) then permits an analytic determination of the secondary electron distribution (Eq.3.4). With these approximations, it is then possible to calculate the energy converted into the j^{th} state via the secondary, tertiary, etc., electrons by the solution of a rather simple integral equation. We refer the reader to the details of the papers based upon this technique.

4(b) Soft Electron Fluxes and Electron-Electron Loss

It was noted in Section 2 that soft electron fluxes (<a few kev) are an important source of energy over the cap. Eather and Akasofa (30) , based on Rees' (49) calculations, note that energy deposition by the soft morning fluxes should be important between 150 and 220 km. Over this altitude range, the relative composition of the neutral species is changing significantly as is the loss to e-e scattering. With increasing altitude, atomic oxygen is becoming the dominant species while e-e loss is becoming the dominant loss process below 5 ev. The main effects we wish to consider arise from composition change and change in the primary energy. The

spatial aspects of the electron loss process is an extremely difficult problem, in fact, impossible without detailed knowledge of all important collisional cross sections. Rather than attempt to solve this problem, we consider an electron of given primary energy and perform a calculation of its degradation at various altitudes. For a given energetic electron, at say, 120 km, the assumption of local loss is fairly reasonable. The assumption, of course, becomes less valid with increasing

altitude. Nevertheless, it is interesting to consider the changes in the local loss process with increasing altitude and as we will see, trends can be pointed out that should relate to the real problem.

In past work [e.g., Green et al (55)], results have been presented in the form of intensities for the various spectral lines and bands based on a scaling technique utilizing measured intensities of the N_2^+ 3914A band. From an atomic point of view, perhaps a more appropriate presentation of electron loss results would be in the form of efficiencies. We define the efficiency for loss to a given process as the fraction of primary energy going to that process. We designate this as $P(E_p)$ and note that loss is included for both primary and secondary electron impact.

We choose to present and compare $P(E_p)$ for a number of important discrete and ion states at sample altitudes of 80, 120, and 250 km. Prior to this, however, we briefly consider the process of e-e loss which at an altitude such as 250 km is the dominant loss below about 5 ev.

The problem of the degradation of low energy electrons in a plasma has been considered by Butler and Buckingham (56), and many others in connection with relaxation time

estimates. Butler and Buckingham have specifically considered the problem in a manner which finds ready application to the problem at hand. Prior application of the Butler-Buckingham approach to the photoelectron dayglow problem has been made by Dalgarno et al (57). It can be shown by the work of Butler-Buckingham that the rate of electron-electron energy loss associated with elastic collisions considerably exceeds the rate of electron-ion energy loss. Accordingly, we shall concentrate our attention on the former mechanism. For this problem the work of Butler-Buckingham may be placed in the form

$$\frac{dE}{dx} = -n_e \frac{4\sqrt{\pi}}{E} e^4 \left(\frac{v}{\omega_t}\right) F \left(\frac{v}{\omega_t}\right) \ell n \Lambda \tag{4.5}$$

where ω_t is defined in terms of the thermal energy W_t by

$$W_t = \frac{3}{2} kT = \frac{3}{2} \left[\frac{m\omega_t^2}{2}\right] \tag{4.6}$$

$$F(x) = \frac{1}{x} \int_o^x \exp(-x^2)\, dx - 2 \exp(-x^2) \tag{4.7}$$

and $\Lambda = 2/\theta_0$ where θ_0 is the minimum angle of scattering corresponding to a Coulomb collision at an impact parameter equal to the Debye shielding distance. The function F(x) may be approximated by

$$F(x) \approx \frac{\sqrt{\pi}}{2} \frac{1}{x} \left(1-\frac{1}{x^2}\right)^{\nu} \quad ; \quad \nu \approx 1/2. \tag{4.8}$$

Using the usual expression for Rutherford scattering and the formula for the Debye length the factor Λ can be shown to be given approximately by

$$\Lambda = 2/\theta_0 = \frac{2E}{e^2} \left(\frac{kT}{4\pi ne^2}\right)^{1/2} \approx E\left(\frac{T}{ne}\right)^{1/2} 3 \times 10^6 \tag{4.9}$$

where in the last expression E is in eV, T is in 10^3K and n is in 10^6/cc.

We may finally gather our results and approximations together to obtain an electron-electron energy loss in the form used by Green and Barth (34)

$$L_e = A_e \frac{q_0}{E} \left(1-\frac{W_t}{E}\right)^{\nu} \tag{4.10}$$

where

$$A_e = 2 \ln \left(\frac{2}{\theta_0}\right) \approx 30 + \ln (E^2T/ne) \tag{4.11}$$

is an effective strength for e-e collisions. This result has been used by Stolarski (50) with the constants $W_t = 0.15$ and $A_e q_o = 1.95 \times 10^{-12}$. The latter constant agrees with the approximation Dalgarno et al. (57) use above 3 eV. The factor $[1-(W/E)]^{\gamma}$ can be replaced by the form $1-(W/E)^{\Gamma}$ to bring into our current standard form. Accordingly, the inclusion of e-e loss mechanisms presents no serious complication in our analysis.

4(c) EFFICIENCIES

In figure 5, we present a breakdown of the primary energy into its various gross loss channels. The efficiencies to be presented refer to those channels above the dividing line shown in the figure. For a given excited state, we thus consider the fraction of the original primary energy transformed by electron impact alone, which includes however, primary and secondary, electron impacts. As indicated in the figure, if one wishes to carry the problem further, he must then apply chemistry to determine the fate of the considerable quantity of potential energy carried by the ions.

In figs. 6-8, we present selected efficiencies at the altitudes of 80, 120 and 250 km. We may place these in the following catagories: 1) electronic state excitation, 2) total ionization for each species as well as the sum for all species and 3) combined vibrational and e-e loss (low energy processes). The model densities, both neutral and electron, as well as the electron temperature for these altitudes are given in Table 1. All such parameters determine the energy loss variations which arise in altitude changes. The electron densities and temperatures are meant to correspond to the polar ionosphere during very weak auroral activity.

To arrive at the given efficiencies, we have applied the techniques of electron degradation already discussed. The applied loss function at the various altitudes contains cross sections for some 200 electronic states of O , O_2 and

N_2 as well as cross sections for vibrational states and for loss to ambient electrons. With only minor modifications, the electronic state cross sections used are those appearing in Peterson et al. (58). Because we are presenting only selected efficiencies, their sum, of course, will not total to 100%. We require, however, 100% for all processes represented in our loss function to preserve conservation of primary energy.

In the figures, the efficiencies are represented as functions of the primary electron energy E_p which spans a range from 1 to 1000 ev. A word of caution should be made regarding energies below about 50 ev. As described earlier, a continuous slow down approximation has been used and based on Peterson's (59) recent work, errors of the order of 25% below 50 ev can be expected for some states based on this assumption. Another difficulty inherent in the problem is the greater uncertainty in cross sections near threshold. Nevertheless, it is interesting to consider the low energy region, in particular, because of the increased importance of vibrational, rotational and e-e loss. We might also single out the $a^1\Delta g$ state of O_2 because of its low threshold of .98 ev and the considerable interest recently directed towards its possible sources of excitation in the atmosphere.

One of the first things we note is the insensitivity of nearly all efficiencies above 100 ev. This arises simply from the similar behavior of most impact cross sections above this energy. In the region between 100 ev and 50 ev, a general

trend is for excitation efficiencies to increase and ionization efficiencies to decrease. Such a behavior has been pointed out earlier by, e.g., Stolarski and Green (60) and simply reflects the enhancement in discrete excitation as competition with ionization diminuishes. In the region below 10 ev, where few electronic states possess sizable cross sections, most of the efficiency goes to vibrational, rotational and e-e loss. Of the electronic states which do contribute, the most important at, e.g., 120 km are O_2, $^1\Delta g$ and OI ^1S with thresholds respectively at .98 and 1.9 ev.

Having pointed out some general trends, let us next consider ionization efficiencies. In all cases above 500 ev, over 50% of the primary energy is transferred to potential energy carried by the ions. If we were to add to this, the initial kinetic energy carried off by the ejected electrons, we see that well over half of the primary energy goes to the process of ionization. We do not show the amount of kinetic energy carried by the secondaries, however, since we have applied the loss calculation to these as we have to the primary. Their energy is thus distributed among all energetically available states. Considering ionization for each species, we first note that the O^+ efficiency dominates at 25.0 kv and is insignificant by the time we reach 80 km. At the altitudes considered, the N_2^+ efficiency is always a significant fraction and comprises most of the total ionization efficiency at 80 km. These effects basically reflect the changes in relative concentration of the gases (see Table 1).

Referring back to Fig. 5, we note how important chemistry is, considering that approximately half of the primary energy (for primaries above a few hundred ev) is directly transferred to potential energy in the ion states. At higher altitudes such as 250 km, ion diffusion is also an important factor in the eventual fate of the ion energy.

The 3914 band is particularly important as a photometric standard in aurora and dayglow intensity measurements. We have included its efficiency at each altitude. We wish to note, however, that this efficiency or fraction of primary energy includes the ionization energy of the N_2^+ ground state (15.5 ev) as well as the actual 3914 band energy (3.17 ev). Fig. 9 shows the 3914 production cross section according to various measurements [we include McConkey et al. (61) and Borst and Zipf (62)]. In this present work we have refit the integrated cross section associated with the differential cross section equation given by Eq. 4.4 to the most recent data [Borst and Zipf (62)]. The reassigned parameters are

$$A_o = ,246 \quad \Gamma_1 = .152 \quad P = 1.2 \quad a_o = 1 \quad a_1 = -1 \quad \Gamma_o = 0$$

We have also use the ionization cross section with

$$\sigma = \frac{A_o}{\nu(E + K)} \ln\left[\left(\frac{E - I}{J}\right)^{\nu} + 1\right] \qquad 4.12$$

The parameters $A_o = 20.2$, $\nu = 1.2$, $K = 13.1$ and $J = 89.1$ give the fit to the data shown by the dashed curves in Fig. 9. This latter equation is a simple, versatile form which might be applied to any ionization cross section from threshold to the E^{-1} lnE region of the Born approximation.

For excitation to the $N_2^+ B^2\Sigma_u^+$ state leading to 3914 emission at, e.g., 80 km, we obtain an efficiency of about 2.7% for Ep = 1000 ev. Taking the ratio of 3914 A energy to the excitation energy of the $^2\Sigma_u^+$ state, i.e. 3.17/18.75, we obtain an efficiency of .46 for the 3914 Å band. We note that this is somewhat higher than a value of .34 obtained by Hartman (63) at Ep = 700 ev for similar concentrations.

Turning to the efficiencies of specific states and comparing figs. 6-8, the differences, for the most part, reflect the changes in relative concentrations from one altitude to another. In particular, from 120 km to 250 km, efficiencies for states of OI with thresholds of several ev have increased roughly by a factor of seven in agreement with the relative increase of OI. It is interesting to note, however, that the low threshold state OI ^1D (1.92 ev) has increased by less than a factor of two. This is attributed to the fact that most ^1D excitation is produced by secondaries in the low energy region where very few other states contribute to the energy loss. Thus, the ^1D state contributes significantly to the loss function at low energy and its contribution does not vary in proportion to the relative composition of OI.

In figs. 6-8, we have indicated the fraction of energy transferred to vibrational excitation and e-e loss. At 1 kev, the values range from about 7% to 9%. This amount arises

almost entirely from secondary electron loss. The secondary spectrum itself is weighted heavily below say 50 ev. We note that the largest value occurs at 250 km. The magnitude itself strongly depends on the effectiveness of other excitation processes in competing below 10 ev. At 250 km, only the OI ^1D state is a competitor and then only above about 5 ev. At 120 km, OI ^1D is still important but also included now is O_2 $a^1\Delta_g$ (1.27μ emission). For the given relative concentrations and assumed cross sections, competition is greater at 120 than at 250 km thus producing a smaller efficiency with decreasing altitude. The magnitude we have chosen for the $^1\Delta_g$ cross section is based on the data of Hake and Phelps (64).

It is interesting to consider the 1.27μ/3914A ratio which has been reported to reach large values in recent studies [Noxon et al (65) and Megill (personal communication)]. If the stimulating mechanism consists of very low energy electrons (25eV) this ratio can become arbitrarily large not so much because 1.27 becomes large but rather that 3914 becomes small. This should be obvious from Fig. 6, 7, and 8. A more detailed treatment of this problem has been given by Prasad et al. (66).

In this section, we have presented results of electron degradation in the form of efficiencies and have pointed to effects which arise as we change the altitude and primary energy. The discussion has been rather general with no special emphasis on polar cap phenomena. We would relate the above discussion to such phenomena, in particular, to soft flux deposition by analysing our results from say 120 to 250 km over a range of primaries from say 1000 down to 100 ev or less.

5. Processes Stimulated by Protons

(a) Overview

As yet, there have been no studies of the energy deposition of protons, which have been carried out with the degree of microscopic detail which has been applied to electrons (as discussed in the previous section). The state of knowledge of the proton impact cross sections in the low energy region lags considerably behind the state of knowledge of electron impact cross sections.

With the growth of interest in atomic collisions this condition might change rapidly. Hence, one might anticipate that experimental data will be forthcoming before long upon which to base a semi-empirical approach similar to that used in the previous section. Another obstacle to the development of a microscopic approach to proton degradation is the somewhat greater complexity occasioned by the charge changing processes. To illustrate this complication, let us consider the various processes which play a role, for example, in the slowdown of a proton in a neutral molecular nitrogen.

Figure 10 illustrates the various processes that can occur. Reaction 1 is a process leading to the vibrational or electronic excitation of nitrogen. Reactions 2 and 3 lead to single ionization and double ionization. Reaction 4 leads to

molecular dissociation. Each of these reactions are directly analogous to the corresponding reactions induced by electrons. Indeed, there are scaling laws based upon the Born-Bethe approximation which relate the two sets of cross sections at high energies. However, reactions 5 - 7 through various types of charge exchange reactions which lead to the neutralization of the proton or to negative hydrogen ion formation, have no parallels in the electron degradation process. Now, here it must be noted that the consequence of such reactions which generally do not require very much energy exchange is a rapidly moving neutral hydrogen atom, which may, in many instances, be in an excited state. Accordingly, we must also consider the fate of these neutral hydrogen atoms in the atmosphere. Reactions 9, stripping, and 10, stripping and ionization, represent the two most likely processes which can occur in fast hydrogen atom nitrogen collisions.

It should be noted that any of reactions 5 through 7, when followed by any of reactions 9 through 11, constitutes a complete charge changing cycle. Thus, two such processes, together, act in

a very similar way to a single electron impact loss process in the sense that the outcome now is a proton which has less energy than the incident proton. Accordingly, if one knows the cross sections for 5, 6, and 7, and for 9, 10, and 11, one could, in principle, assign net cross sections for the combined processes as well as an approximate net energy loss suffered by the incident proton.

Eq. 8, the process of double capture, generally has rather small, but not insignificant, cross sections. This double capture can then be followed by a stripping which leads to a neutral hydrogen or by double stripping, which leads again to protons. In the former case, the hydrogen can proceed via 9, 10, or 11 back to protonic form. It should be clear that, if we know all the cross sections involved in a complete charge change cycle, one could establish net cross sections and net loss functions for the various series of processes in which a proton returns to a proton with a net energy loss.

At low energies (<10 keV) elastic collisions leading to transfer of kinetic energy to other atoms become a major loss mechanism. Let us assume that all the cross sections of protons, hydrogen atoms, and negative hydrogen ions are known, say, from the 10 MeV region down to the 500 eV region. The net consequence of a primary proton degrading to these low energies is

the conversion of the proton energy to ionized nitrogen, excited nitrogen, dissociation, and the kinetic energy of secondary electrons. Accordingly, it should be feasible if the systematics of the cross sections in Fig. 10 were known, to attempt for protons the types of calculations discussed in the previous section when electrons served as the stimulating mechanism.

In a recent work of Green and McNeil, (67) semi-empirical analytic forms are applied to proton and hydrogen ionization and capture and charge-changing collisions. This work encourages one to think that the goal discussed above might be reached in the relatively near future. At this point, we can only outline the essential aspects of the calculation of proton-stimulated spectral emissions without presenting quantitative results.

The steps, which one must become involved with in this type of calculation are illustrated in Fig. 11. Again, we first must know the incident proton flux. These usually involve two types, one being the high energy proton fluxes associated with intense solar activity, which at the same time are usually accompanied by very disturbed magnetic fields.

Such events, of course, play an important part in the polar cap region as well as in the normal auroral zone itself. In addition, one also has the flux associated with regular solar wind, whose characteristics are not too well-known, particularly insofar as its neutral component. We next must concern ourselves with the geomagnetic influence upon the geometry of proton motion (2). Protons are only guided by the magnetic field lines. When they capture a charge they become decoupled from the magnetic field lines and travel in straight paths. Then, upon stripping, these fast moving particles become recoupled again. This diffusion of the protons with respect to field lines represents a complicated aspect of the positive ion problem, which, of course, electrons do not experience.

When the protons or hydrogen atoms reach the lower altitudes where the interactions become important, we must know the altitude distribution of the atmospheric species (3), where the interactions play an important role.

The degradation, penetration, and straggling problem of the proton and neutral hydrogen atoms (4) is quite different from those of low energy electrons. Because of their larger momenta, protons do not straggle as greatly, even at lower energies. To deal in detail with such calculations, we must know the charge exchange ionization, secondary electron production, and other collisional cross sections for the processes referred to in Fig. 10. If these are known, one should be able to apportion the incident proton energy into the various forms, secondary electron energy, ionization, and direct excitation. At this juncture, the problem again becomes directly analogous to the electron impact problem since the further degradation of the low-energy secondary electrons would proceed just as in the cases of photon or electron stimulated processes discussed in Section 2 and 3.

Accordingly, we see that, by virtue of the progress with the electron degradation problem using the microscopic approach, we are now entering the phase where the proton degradation problem should be tractable in a similar way. This conjecture is supported by the fact that we also have good data on proton energy loss functions by direct measurement, which can be compared with the loss functions built up from a microscopic viewpoint.

Most critically, however, is the recent availability of experimental results which lead to the spectra of secondary electrons produced by primary protons impacting upon various gases. [Rudd (68), Anderson (69), and Kuyatt and Jorgenson (70)]. When this type of data is represented in some semi-empirical form and systematized so as to be consistent with observed total cross sections and total loss functions it should be possible to pursue the problem of calculating proton stimulated emissions in a directly analogous way to electron stimulated emissions. This work, however, remains to be done in detail.

(b) The Degradation Problem

A key step in the translation of electron energy degradation techniques to protons is the availability of good representations of overall proton loss functions. The results of Green and Peterson (54) may be placed in the form

$$L(E) = \frac{(Za)^{\Omega} E^{\nu}}{J^{\Omega+\nu} + E^{\Omega+\nu}} L_o \qquad (5.1)$$

Here, E is the proton energy, Z is the number of electrons in an atom of the target gas, a and J are characteristic energies (in KeV), Ω and ν are characteristic dimensionless constants and L_o a convenient unit of loss, (e.g. 10^{-15}cm^2 ev). In the absence of detailed data, we may take $\Omega \approx 0.75$, $\nu \approx 0.6$, a = 1510 KeV, J = 83 KeV as a general rule. However, for greater accuracy, we should use individual loss function constants. The loss function constants for several of the atmospheric gases are given in Table 2.

The work of Green and McNeal (67) indicates that if L_o is replaced by σ_o Eq. (5.1) can also be used to represent proton and hydrogen cross sections with good accuracy over a broad energy range. The constants a, ν, and Ω for proton ionization, hydrogen ionization, hydrogen stripping, and charge capture by protons and hydrogen, all show a fairly regular behavior. Furthermore, it appears that one can relate the constants for proton and neutral hydrogen ionization to constants obtained by fitting electron ionization. The work suggests that one can relate proton excitation cross sections to electron excitation cross sections in a similar way. The recent availability of experimental results which lead to the spectra of secondary electrons produced by primary protons impacting upon various gases offers further encouragement to the microscopic approach. When this type of data is represented in some semi-empirical form and systematized so as to be consistent with observed total cross sections and total loss functions it should be possible to pursue the problem of calculating proton stimulated emissions in a directly analogous way to electron stimulated emissions.

To illustrate this view more concretely, let us consider in greater detail how we might treat charge changing cycles. For example, following the process 5 listed in Fig. 10 we might have process 9, leading to the net reaction

$$H^+ + 2N_2 \rightarrow H^+ + N_2^{+(i)} + N_2^{(j)} + e + \Delta E \qquad (5.2)$$

Alternatively, 5 might be followed by 10 leading to the net reaction

$$H^+ + 2N_2 \rightarrow H^+ + N_2^{+(i)} + N_2^{+(j)} + 2e + \Delta E \qquad (5.3)$$

Again, 5 might be followed by 11, leading to the net reaction

$$H^+ + 2N_2 \rightarrow H^+ + N_2^{+(i)} + N_2^{++} + 3e + \Delta E \qquad (5.4)$$

Such a scheme may be carried through all nine possible net reactions possible with processes 5, 6, 7 and 9, 10, 11; and similarly for processes 8 and 15.

Now, net cross sections and energy loss functions may be assigned to each of the separate "combined" processes. It should be clear that if we know all the cross sections involved in a complete charge changing cycle, one could establish net cross sections and net loss functions for these processes.

Following recent work by Green and McNeal, in which semi-empirical analytic forms describe the proton and hydrogen ionization capture, charge changing interaction cross sections, a preliminary investigation has been started on the proton degradation problem. We present here an outline of the present, initial, study. In an effort to incorporate previous work with electrons and also treat a major channel through which energy losses occur, we treat the secondary electron distribution arising from the complete degradation of a primary energy E_p.

It has become apparent that the secondary electron distributions due to proton slowdown may be characterized by simple functions, to within a reasonable approximation. Now, we denote by $n(E_p,T)$ the fraction of secondary electrons with kinetic energy between T and T + dT resulting from the degradation of an incoming proton with initial kinetic energy E_p. We have explored a variety of functional representations including the separable forms

$$n(E_p, T) = F_1(E_p)F_2(T) \tag{5.5}$$

The types of functions investigated for F_1 include functions such as

$$F_1 = E_p^2/A(E_p + J) \tag{5.6}$$

For F_2 we have looked at

$$F_2 = (J^\nu + T^\nu)^{-1} \quad (5.7) \qquad F_2 = (J + T)^{-\nu} \quad (5.8)$$

and

$$F_2 = [(e^{\alpha t} - 1)\eta + 1]^{-1} \quad (5.9)$$

Eqs. (5.7) and (5.8) go over to the ordinary power law when $J \to 0$. Eq. (5.9) goes over to the ordinary exponential law when $\eta \to 1$. Each of these equations has advantageous analytic features, and at the same time may be used to represent integral or differential spectra quite well.

We have given more detailed attention to a double exponential form suggested by experimental observations. In particular, we have used the form

$$n(E_p, T) = [E_p^2/A(E + J)]e^{-T/L} + [E_p^2/B(E + K)]e^{-T/H} \quad (5.10)$$

where L = 8 eV, H = 32 eV, A = .256 KeV, B = 4096, and $J \approx 1$ KeV, $K \approx 100$ KeV.

This distribution with these constants has the property that at high energies ($E_p >> K$) 25% of the proton energy goes into the high energy spectrum. At intermediate energies $J<E<K$ the high energy component remains. At low energies ($E< J$) the low

energy component also fades out. This form seems capable of encompassing all facts presently known. It provides a convenient electron spectrum which can be fed directly into the electron degradation program.

We can also attempt a more microscopic approach if we can find reasonable representations of the differential ionization cross sections for protons. Let the differential cross sections be denoted by

$$S(T, E) = S_o f(T/G) \left(\frac{T}{E}\right)^{\Omega} \tag{5.11}$$

where G, the "ionization energy", is given by

$$G = G_o \left(\frac{E}{B}\right)^{\nu} / \left[1 + \left(\frac{E}{B}\right)^{\nu}\right] \tag{5.12}$$

A variety of f(x) may be used, but the studies of Rudd (68) and Anderson (69) suggest

$$f(x) = a\, e^{-\alpha x} + (1-a)\, e^{-\nu\alpha x} \tag{5.13}$$

Now we can adjust our parameters by insuring that these parameters correspond to the total ionization cross sections such as those of Green and McNeal. We may use (discounting ionization energy)

$$\sigma(E) = \int_o^E S(E, T)\, dT \tag{5.14}$$

Once we have these parameters we obtain an analytic proton loss function for the given process under study by using

$$L(E) = \int_0^E TG(E,T)\,dT \qquad (5.15)$$

Again, we may usually discount the relatively small ionization energy. With this more microscopic approach we can attempt to derive net loss functions associated with average ionization process.

This primative approach whose usefulness depends upon the accuracy of estimates of the parameters A, B, J, K and L and H provides a detailed characterization of the portion of primary energy which goes into secondary electrons. With a reasonable prescription for the average energy necessary to ionize a species, it is possible to estimate the energy which goes into the ions. The balance goes into excitation, dissociation, and other processes. Estimates of this balance can be obtained from net proton loss functions Eq. (5.1).

To truly parallel our microscopic electron degradation calculations, we must assign a proton differential ionization cross section for each ionization continua. There is relatively little direct data upon which to base such assignments as yet.

However, one might be able to translate differential cross sections for electrons to protons by use of simple rules.

For the discrete states excited directly by protons we can treat the problem in the same manner in which the electron discrete states are treated. By use of these methods we can now start to do the actual calculations necessary for an initial examination of proton aurorae, PCA events, and other proton induced atmospheric phenomena.

Davidson has considered the charge exchange mechanism which permits particles to cross field lines in connection with a Monte Carlo calculation of proton induced auroras. The most effective charge exchange process at high altitudes for protons is the

$$H^+ + O \rightarrow H + O^+$$

Davidson deduced the latitudinal distribution of hydrogen line intensity and the calculations revealed clearly how charge exchange spreading of proton beams may cause diffusions of the order of 100 kilometers or more. We refer the reader to attempts at dealing with the basic mechanisms in this problem by Davidson (71), Prag et al. (72) and Aether (73).

6. Conclusions

In this work we have concentrated on processes induced by photons, electrons and protons. We have reached a relatively high state of understanding on photon induced processes, in connection with the studies of the formation of the ionosphere and the dayglow. Our understanding of electron induced processes has also matured greatly in the last decade in our ability to relate fundamental atomic physics to its atmospheric consequences. Our understanding of proton induced processes is in a much more primitive state largely because of charge exchange processes which occasion great complications. However, from the discussions in section 5 we believe that it should not be too long before the proton induced processes can be dealt with in a way somewhat similar to our approach to electron induced processes.

We should also consider processes induced by heavy particles and general atmospheric collisional processes particularly at low energies. Here we must recognize that the numerous chemical reactions which occur in the atmospheric phenomena can be looked at either from the point of view of a reaction characterized by a rate constant or the more fundamental point of view of a collision characterized by a cross section [J. Ross and E. F. Greene, (74)], [Green and Wyatt, (75)].

One can identify a reaction rate with the collisional cross section for a bimolecular reaction using the equation

$$R = \frac{(2\beta)^{3/2}}{(\pi\mu)^{1/2}} \int_0^\infty \sigma(E)\, E e^{-\beta E}\, dE \qquad (6.1)$$

where $\beta = 1/kT$ with k the Boltzmann constant, T the temperature, μ the reduced mass of the reactants and $\sigma(E)$ the reactive cross section. Here one can see an advantage of an analytic approach to cross sections. For example if we assume that the reaction cross section has the form

$$\sigma(E) = 0 \quad E < E_\alpha \quad ; \quad \sigma(E) = [f(E - E_\alpha)]/E \quad E > E_\alpha \qquad (6.2)$$

it follows that

$$R(\ ) = \frac{(2\beta)^{3/2}}{(\pi\mu)^{1/2}} e^{-\beta E_\alpha} \int_0^\infty f(x)\, e^{-\beta x}\, dx \qquad (6.3)$$

where $x = E - E_\alpha$. Thus we see that, apart from coefficients, the reaction rate is the Laplace transform of the collisional cross section.

Now there are enumerable reactions which occur in the upper atmosphere which relate to the problems of the aurora dayglow and the ionosphere. Such reaction rates must eventually be related to collisional cross sections. However these subjects are so vast that we can not here attempt to summarize or relate them to each other. It seems clear however, that once the systematics of proton cross sections are established it should be possible to use this systematics to extrapolate the cross sections for heavier particles. This step would

represent a much smaller extrapolation than say from electrons to protons. Here the recent work of Green and McNeal (67) on the systematics of proton and hydrogen inelastic cross sections, should serve as a guide towards the estimation of collisional processes in the upper atmosphere induced by heavier particles.

The writers would like to thank L. R. Peterson and S. S. Prasad for many helpful discussions. One of us would also like to thank Drs. H. W. Hoerlin and M. H. Peek of the Los Alamos Scientific Laboratory and Drs. G. A. Paulikus and R. J. McNeal at Aerospace Corporation for their hospitality last summer when portions of this work were written. They would also like to thank T. C. Pewitt, C. Pittman, M. Bryant, and I. Mitchell for assistance in calculations and preparation of the manuscript.

This work is supported by a grant from the National Aeronautics and Space Administration NsG-599.

References

1. R. J. Mackin and M. Neugebauer, The Solar Wind, Pergamon Press, 1966. (Proceedings of a Conference held at the California Institute of Technology, Pasadena, Calif., April 1-4, 1964)

2. N. F. Ness, "The Earth's Magnetic Tail," J. Geophys. Res., Vol. 70, pp. 2989-3005, 1965.

3. W. I. Axford, H. E. Petschek, and G. L. Siscoe, "Tail of the Magnetosphere," J. Geophys. Res., Vol. 70, pp. 1231-1239, 1965.

4. S. J. Bame, J. R. Asbridge, H. E. Felthauser, E. W. Hones, and I. B. Strong, "Characteristics of the Plasma Sheet in the Earth's Magnetotail," J. Geophys. Res., Vol. 72, pp. 113-129, 1967.

5. M. D. Montgomery, S. Singer, J. P. Conner and E. E. Stogsdill, "Spatial Distribution, Energy Spectra, and Time Variations of Energetic Electrons (E > 50 keV) at 17.7 Earth Radii," Phys. Rev. Letters, Vol. 14, pp. 209-213, 1965.

6. E. W. Hones, Jr., "Observations in the Magnetotail and Their Interpretation," Atmospheric Emissions (Proceedings of the NATO Advanced Study Institute, July 29-August 9, 1968), Ed. B. M. McCormac and A. Omholt, Reinhold Book Corp., New York, 1969.

7. E. W. Hones, Jr., S. J. Bame, S. Singer, and R. R. Brown, "Observed Correlations between Electron Bursts in the Magnetotail and Electron Precipitation in the Auroral Zone," J. Geophys. Res., Vol. 73, pp. 6189-6199, 1968.

8. B. N. McCormac and A. Omholt, Atmospheric Emissions (Proceedings of the NATO Advanced Study Institute), Reinhold Book Corp., New York, 1969.

9. G. Reid, "Particles and Radiation," J. Franklin Institute (this volume).

10. Y. Hakura, "Mapping of the Polar Cap Ionosphere by Solar and Magnetospheric Particles," J. Franklin Institute (this volume).

11. R. G. Johnson and R. D. Sharp, "Satellite Measurements on Auroral Particle Fluxes," Atmospheric Emissions, Ed. B. M. McCormac and A. Omholt, Van Nostrand Reinhold Co., New York, 1969.

12. J. L. Burch, "Low-Energy Electron Fluxes at Latitudes above the Auroral Zone," J. Geophys. Res., Vol. 73, pp. 3585-3591, 1968.

13. R. A. Hoffman and D. S. Evans, "Field Aligned Electron Bursts at High Latitudes Observed by OGO4," J. Geophys. Res., Vol. 73, pp. 6201-6214, 1968.

14. R. A. Hoffman, "Low-Energy Electron Precipitation at High Latitudes," J. Geophys. Res., Vol. 74, pp. 2425-2432, 1969.

15. B. N. Maehlum, "Universal-Time Control of the Low-Energy Electron Fluxes in the Polar Regions," J. Geophys. Res., Vol. 73, pp. 3459-3468, 1968.

16. I. B. McDiarmid and J. R. Burrows, "Electron Fluxes at 1000 Kilometers Associated with the Tail of the Magnetosphere," J. Geophys. Res., Vol. 70, pp. 3031-3044, 1965.

17. J. E. McCoy, "High-Latitude Ionization Spikes Observed by the POGO Ion Chamber Experiment," J. Geophys. Res., Vol. 74, pp. 2309-2318, 1969.

18. B. J. O'Brien, "Rocket and Satellite Observations of Energetic Particles During P. C. A. Events," Space Research VII, Ed. R. L. Smith-Rose, S. A. Bowhill and J. W. King, North Holland, Amsterdam, pp. 806-818, 1967.

19. A. L. Vampola, "Energetic Electrons at Latitudes above the Outer-Zone Cutoff," J. Geophys. Res., Vol. 74, pp. 1254-1269, 1969.

20. K. Lassen, "Polar Cap Aurora," Aurora and Airglow, Ed. B. M. McCormac, pp. 453-464, 1967.

21. A. I. Akasofu, "Dynamic Morphology of Auroras," Space Sci. Rev., Vol. 4, pp. 498-540, 1965.

22. B. P. Sandford, "Polar-glow Aurora in Polar Cap Absorption Events," J. of Atmosp. Terr. Phys., Vol. 24, pp. 155-171, 1962.

23. J. B. Blake, G. A. Paulikas, and S. C. Freden, "Latitude-Intensity Structure and Pitch-Angle Distributions of Low-Energy Solar Cosmic Rays at Low Altitude, J. Geophys. Res., Vol. 73, pp. 4927-4934, 1968.

24. G. A. Paulikas, J. B. Blake, and S. C. Freden, "Low-Energy Solar-Cosmic-Ray Cutoffs: Diurnal Variations and Pitch-Angle Distributions," J. Geophys. Res., Vol. 73, pp. 87-95, 1968.

25. K. Lassen, "Polar Cap Emissions," Atmospheric Emissions, Ed. B. M. McCormac and A. Omholt, Van Nostrand Reinhold Co., New York, pp. 63-71, 1969.

26. P. B. Sandford, "Variations of Auroral Emissions with Time, Magnetic Activity and the Solar Cycle," J. Atmosp. Terr. Phys., Vol. 30, pp. 1921-1942, 1968.

27. T. N. Davis, "Negative Correlation between Polar-Cap Visual Aurora and Magnetic Activity," J. Geophys. Res., Vol. 68, pp. 4447-4454, 1963.

28. B. P. Sandford, "Polar-Glow Aurora," Space Research VII, Ed., R. L. Smith-Rose, S. A. Bowhill and J. W. King, North-Holland, Amsterdam, pp. 836-843, 1967.

29. T. R. Hartz and N. M. Brice, "The General Pattern of Auroral Particle Precipitation," Planet. Space Sci., Vol. 15, pp. 301-329, 1967.

30. R. H. Eather and S. I. Akasofu, "Characteristics of Polar Cap Auroras," J. Geophys. Res., Vol. 74, pp. 4794-4798, 1969.

31. R. H. Eather, "Latitudinal Distribution of Auroral and Airglow Emissions: The 'Soft' Auroral Zone," J. Geophys. Res., Vol. 74, pp. 153-158, 1969.

32. G. V. Starkov, Geomagnetism in Aeronomy, Vol. Vii, pg. 36 (Russian).

33. H. E. Hinteregger, L. A. Hall, and C. Schmidkte, "Solar XUV Radiation and Neutral Particle Distribution in July 1963 Thermosphere," Space Research V, Ed. D. G. King-Kele, P. Muller and G. Righini, et al., North Holland, Amsterdam, pp. 1175-1190, 1965.

34. A. E. S. Green and C. P. Barth, "Calculations of the Photoelectron Excitation of the Dayglow," J. Geophys Res., Vol. 72, pp. 3975-3986, 1967.

35. A. Dalgarno, M. B. McElroy, and A. I. Stewart, "Electron Impact Excitation of the Dayglow," J. Atmos. Sci., Vol. 26, pp. 753-762, 1969.

36. G. R. Cook and P. H. Metzger, "Photoionization and Absorption Cross Sections of O_2 and N_2 in the 600-1000 A Region," J. Chem. Phys., Vol. 41, pp. 321-336, 1964.

37. D. C. Frost, C. A. McDowell, and D. A. S. Vroom, "Phot-electron Kinetic Energy Analysis in Gases by Means of a Spherical Analyses," Proc. Roy. Soc. London, Vol. 296, pp. 566-579, 1967.

38. R. I. Schoen, "Laboratory Measurements of Photoionization, Photoexciation, and Photodetachrent," Proceedings of the Symposium of Laboratory Measurements of Aeronomic Interest, Ed: H. I. Schiff, pp. 1879-1900, 1969.

39. L. R. Peterson and A. E. S. Green, "The Relation between Ionization Yields, Cross Sections and Loss Functions," Proc. Phys. Soc., Vol. 1B, pp. 1131-1140, 1968.

40. C. A. Barth, "The Ultraviolet Spectroscopy of Planets," The Middle Ultraviolet: Its Science and Technology, Ed: A. E. S. Green, John Wiley and Sons, New York, pp. 177-218, 1966.

41. T. M. Donahue, T. Parkinson, E. C. Zipf, J. P. Doering, W. G. Fastie and R. E. Miller, "Excitation of the Auroral Green Line by Dissociative Recombination of the Oxygen Molecular Ion: Analysis of Two Rocket Experiments," Planet. Space Sci., Vol. 16, pp. 737-747, 1968.

42. S. Chapman,"Note on the Grazing-Incidence Integral Ch(x,χ) for Monochromatic Absorption in an Exponential Atmosphere," Proc. Phys. Soc., Vol. 66B, pp. 710-712, 1953; also see S. Chapman, "The Absorption and Dissociative or Ionizing Effect of Monochromatic Radiation in an Atmosphere on a Rotating Earth," Proc. Phys. Soc., Vol. 43, pp. 26-45, 1931; S. Chapman, "The Absorption and Dissociative or Ionizing Effect of Monochromatic Radiation in an Atmosphere on a Rotating Earth: Part II; Grazing Incidence," Proc. Phys. Soc., Vol. 43, pp. 483-501, 1931.

43. M. V. Wilkes, "A Table of Chapman's Grazing Incidence Integral Ch(x,χ)," Proc. Phys. Soc., Vol. 67B, pp. 304-308, 1954.

44. A. E. S. Green and J. D. Martin," A Generalized Chapman Function," The Middle Ultraviolet: Its Science and Technology, Ed. A. E. S. Green, John Wiley and Sons, New York, p. 140, 1966.

45. A. E. S. Green and P. J. Wyatt, Atomic and Space Physics, Addison-Wesley Publishing Co., Inc., Reading, Mass., pp. 134-135, 1965.

46. G. E. Thomas, "Lyman α Scattering in the Earth's Hydrogen Geocorona, 1," J. Geophys. Res., Vol. 68, pp. 2639-2660, 1963.

47. T. M. Donahue, "Some Considerations Concerning Radiative Transport in the 1304 Triplet in the Upper Atmosphere," Planet, Space Sci., Vol. 13, pp. 871-888, 1965.

48. D. J. Strickland and T. M. Donahue, Excitation and Radiative Transport of the 1304 Resonance Padiation. I. The Dayglow.," in publication, Planet. Space Sci.

49. M. H. Rees, "Auroral Ionization and Excitation by Incident Energetic Electrons," Planet. Space Sci., Vol. 11, pp. 1209-1218, 1963.

50. R. S. Stolarski, "Calculation of Auroral Emission Rates and Heating Effects," Planet. Space Sci., Vol. 16, pp. 1265-1276, 1968.

51. A. E. S. Green and C. A. Barth, "Calculations of Ultraviolet Molecular Nitrogen Emissions from the Aurora," J. Geophys. Res., Vol. 70, pp. 1083-1092, 1965;
A. E. S. Green and S. K. Dutta, "Semi-Empirical Cross Sections for Electron Impact," J. Geophys. Res., Vol. 72, pp. 3933-3941, 1967;
A. T. Jusick, C. E. Watson, L. R. Peterson, and A. E. S. Green, "Electron Impact Cross Sections for Atmospheric Species, I. Helium," J. Geophys. Res., Vol. 72, pp. 3943-3951, 1967;
R. S. Stolarski, V. A. Dulock, Jr., C. E. Watson, and A. E. S. Green, "Electron Impact Cross Sections for Atmospheric Species, 2. Molecular Nitrogen," J. Geophys. Res., Vol. 72, pp. 3953-3960, 1967;
C. E. Watson, V. A. Dulock, R. S. Stolarski, and A. E. S. Green, "Electron Impact Cross Sections for Atmospheric Species, 3. Molecular Oxygen," J. Geophys. Res., Vol. 72, pp. 3961-3966, 1967.

52. M. Gryzinski, "Classical Theory of Electronic and Ionic Inelastic Collisions," Phys. Rev., Vol. 115, pp. 374-383, 1959.

53. A. E. S. Green and R. S. Stolarski, "Electron Impact Excitation of the Ultraviolet," The Middle Ultraviolet: Its Science and Technology, Ed. A. E. S. Green, John Wiley and Sons, New York, pp. 165-176, 1966.

54. A. E. S. Green and L. R. Peterson, "Energy Loss Functions for Electrons and Protons in Planetary Gases," J. Geophys. Res., Vol. 73, pp. 233-241, 1968.

55. A. E. S. Green L. R. Peterson, and S. S. Prasad, "Semi-Empirical Cross Sections and the Airglow and Aurora," Atmospheric Emissions, Ed. M. M. McCormac and A. Omholt, Reinhold Book Corp., New York, pp. 523-532, 1969.

56. S. T. Butler and M. J. Buckingham, "Energy Loss of a Fast Ion in a Plasma," Phys. Rev., Vol. 126, pp. 1-4, 1962.

57. A. Dalgarno, M. B. McElroy and R. J. Moffett, "Electron Temperatures in the Ionosphere," Planet. Space Sci., Vol. 11, pp. 463- , 1963.

58. L. R. Peterson, S. S. Prasad and A. E. S. Green, "Semi-Empirical Electron Impact Cross Sections for Atmospheric Gases," Can. J. Chem., Vol. 47, pp. 1774-1777, 1969.

59. L. R. Peterson, "Energy Deposition of Electrons in Gases by Discrete Steps," in publication, Phys. Rev.

60. R. S. Stolarski and A. E. S. Green, "Calculations of Auroral Intensities from Electron Impact," J. Geophys. Res., Vol. 72, No. 15, pp. 3967-3974, 1967.

61. J. W. McConkey, J. M. Woolsey, and P. J. Burns, "Absolute Cross Section For Electron Impact Excitation of 3914 A N_2^+, Planet Space, Sci., Vol. 15, pp. 1332-1334, 1967.

62. R. F. Holland, "Cross Sections for Electron Excitation of the 3914 A (0,0) Band of the N_2^+ First Negative System," Los Alamos Scientific Laboratory Report #LA-3783, 1967.

63. W. L. Borst and E. C. Zipf, "Cross Section for Electron Impact Excitation of the (0,0) First Negative Bands of N_2^+ from Threshold to 3keV," in publication, Phys. Rev.

64. R. D. Hake and A. V. Phelps, "Momentum-Transfer and Inelastic-Collision Cross Sections for Electrons in O_2, CO, CO_2," Phys. Rev., Vol. 158, pp. 70-84, 1967.

65. I. Isaksen, E. J. Llewellyn and A. V. Jones, Photochemical Effects in the Atmosphere Resulting from Auroral Bombardment, preprint from The Institute of Space and Atmosphere Studies, Univ. of Saskatchewan, Saskatoon, Canada.

66. S. S. Prasad, L. R. Peterson, and A. E. S. Green, in a paper in preparation for future publication.

67. A. E. S. Green and R. J. McNeal, in a paper to be published.

68. M. E. Rudd, Energy and Angular Distribution of Secondary Electrons Produced by 100 keV Protons in Hydrogen and 50-150 keV Protons in Helium, Ph. D. Thesis, Univ. of Nebraska, 1962.

69. J. C. Anderson , Energy and Angular Distribution of Secondary Electrons Produced by 50-200 keV Protons in Nitrogen, Oxygen, Neon, and Argon, Ph.D. Thesis, University of Nebraska, 1965.

70. E. Kuyatt, and T. Jorgenson, Jr., "Energy and Angular Dependence of the Differential Cross Section for Production of Electrons by 50-100 keV Protons in Hydrogen Gas," Phys. Rev., Vol. 130, pp. 1444-1455, 1963.

71. G. T. Davidson, "Expected Spatial Distribution of Low-Energy Protons Precipitated in the Auroral Zones," J. Geophys. Res., Vol. 70, pp. 1061-1068, 1965.

72. A. B. Prag, Fred A. Morse and R. J. McNeal, "Nightglow Excitation and Maintenance of the Nighttime Ionosphere by Low Energy Protons," J. Geophys. Res., Vol. 71, pp. 3141-3154, 1966.

73. R. H. Eather , "Secondary Processes in Proton Auroras," J. Geophys. Res., Vol. 72, pp. 1481-1489, 1967.

74. J. Ross and E. F. Greene, The Study of Chemical Reactions in Crossed Molecular Beams, XII International Solvay Conference, Brussels, Nov. 1962.

75. ibid, Ref. 45, p. 167.

FIGURE CAPTIONS

Fig. 1 Polar cap region defined by high latitude boundary of the visual auroral zone [after Burch (12)].

Fig. 2 Block diagram outlining procedures and quantities needed to derive emission and ionization rates arising from solar XUV radiation.

Fig. 3 Geometry appropriate to the generalized Chapman function as discussed in Section 2.

Fig. 4 Block diagram outlining procedures and quantities needed to derive emission and ionization rates in an aurora for a given incident electron flux.

Fig. 5 Block diagram illustrating the various gross loss channels into which goes the primary electron energy. The efficiencies presented in Figs. 6-8 apply to those channels above the dividing line.

Fig. 6 Efficiencies expressed as functions of primary energy E at 80 km with the appropriate gas concentrations given in Table 1.

Fig. 7 Efficiencies at 120 km.

Fig. 8 Efficiencies at 250 km.

Fig. 9 The 3914A electron impact ionization cross section. Shown are three sets of data [McConkey et al.(61),

Holland (62) and Borst and Zipf (63)] and fits based on the designated equations.

Fig. 10 Reactions involved in a proton slowing down in N_2.

Fig. 11 Proton stimulated spectral emissions (proton auroras).

Table 1. Atmospheric Model Appropriate to Figs. 6-8

Z	n(0)	$n(O_2)$	$n(N_2)$	n_e	T_e(°K)
80	___*	7.95(13)	2.96(14)	___*	___*
120	7.60(10)	7.49(10)	4.00(11)	1.00(5)	1000
250	8.88(8)	2.13(7)	2.86(8)	2.00(5)	1500

*unimportant

Table 2.

Proton Loss Function Parameters for Several Gases.

Species	Ω	ν	a	J
H	0.853	0.667	1180	60
He	0.808	0.672	1150	84
N	0.761	0.589	1300	82
O	0.746	0.594	1380	97
Ne	0.746	0.610	1310	144
A	0.672	0.728	1690	58
Kr	0.586	0.814	2580	56

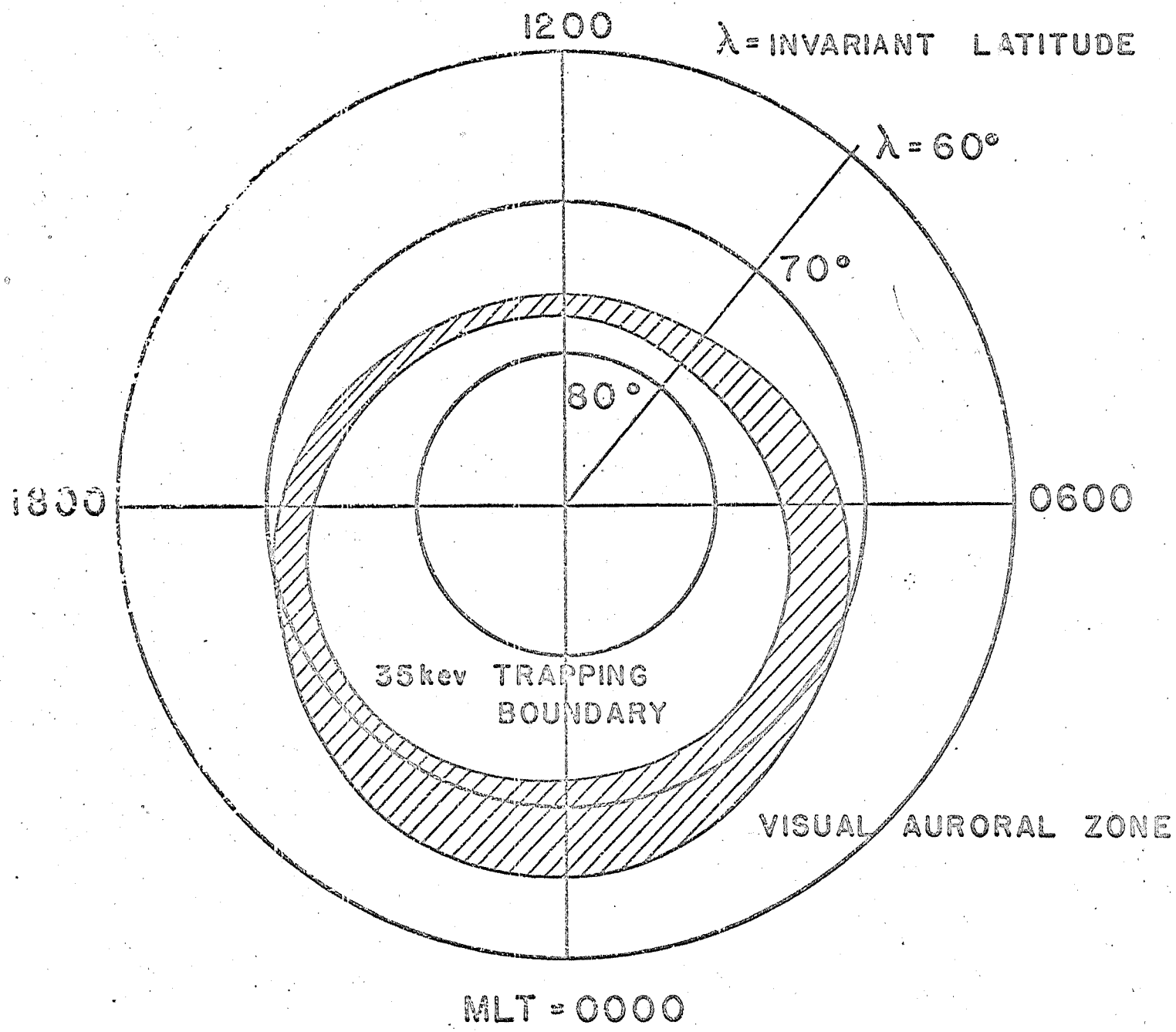

Fig 1, Sharp et al

Fig. 2 Photon Stimulated Spectral Emissions

1. Extreme ultraviolet photon emissions of the sun, iridescence flux, $F_o(\lambda)$
2. Geometry visa vis earth, Chapman Functions
3. Altitude distribution of atomic and molecular species, $n_\ell(y)$
4. Photon absorption cross sections of these species, $\sigma_{ab}(\lambda)$
5. Photo ionization cross sections $\sigma_{ph}(\lambda)$ and $\sigma_{au}(\lambda)$ and photoelectron spectra
6. Electron impact cross sections for excitation, $\sigma_j(E)$, ionization, $S(E,Es)$ and $\sigma_i(E)$, dissociation $\sigma_d(E)$ and other processes
7. Loss function for each species and altitude dependent mixtures $L(E,y) = \Sigma\ L_\ell(E,y)$
8. Primary electron energy transferred to j^{th} state $E_j(E_p)$
9. Primary electron energy transferred to secondary electron spectra, $n_{i\ell}(Es, Ep, y)$
10. Conversion of secondary, tertiary, electron energies to j^{th} state
11. Cascading and brahching in radiative decay
12. Collisional deactivation and other reaction mechanisms
13. Radiative transfer (source to detector)
14. Theoretical result to be compared with experiment
15. FEEDBACK

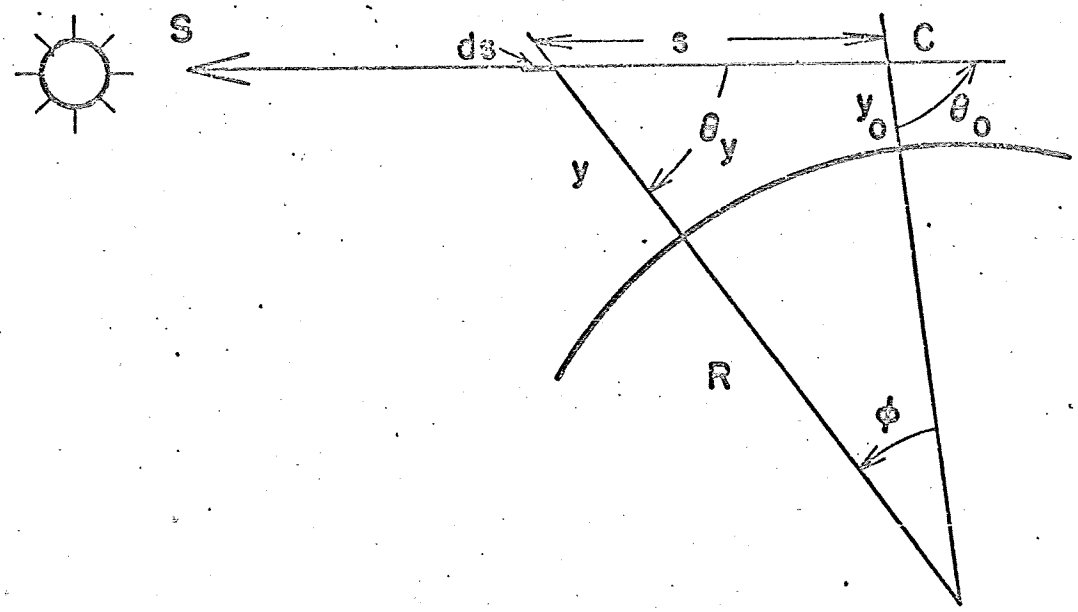
S
ds
s
C
y_o
θ_o
θ_y
y
R
ϕ

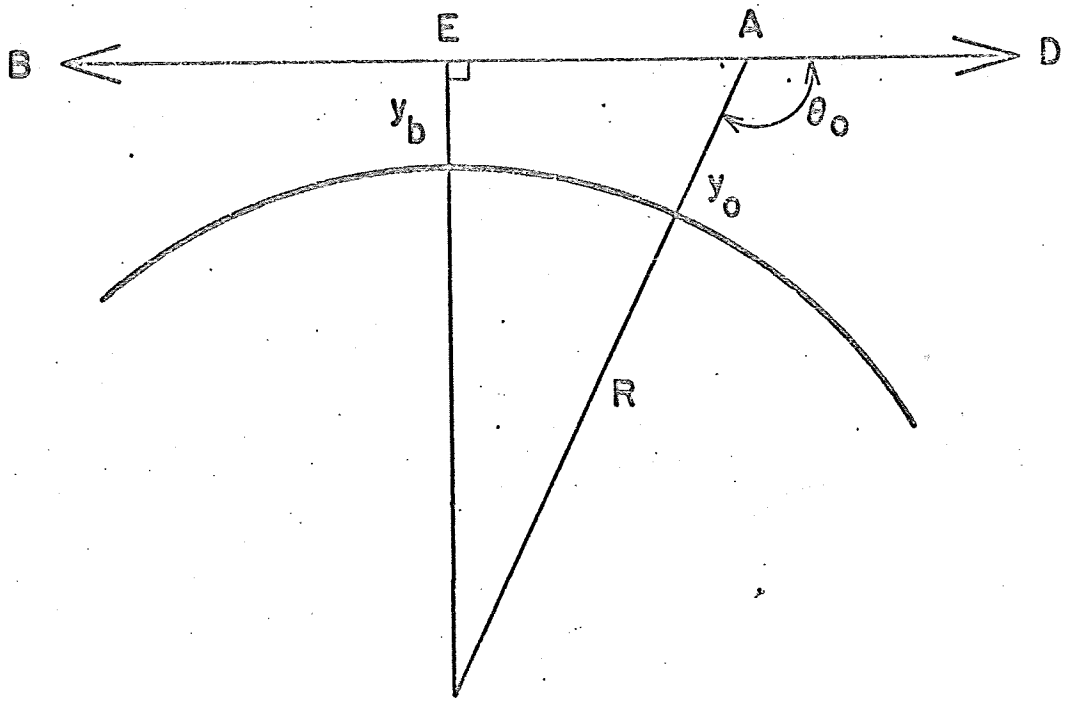
B
E
A
D
y_b
θ_o
y_o
R

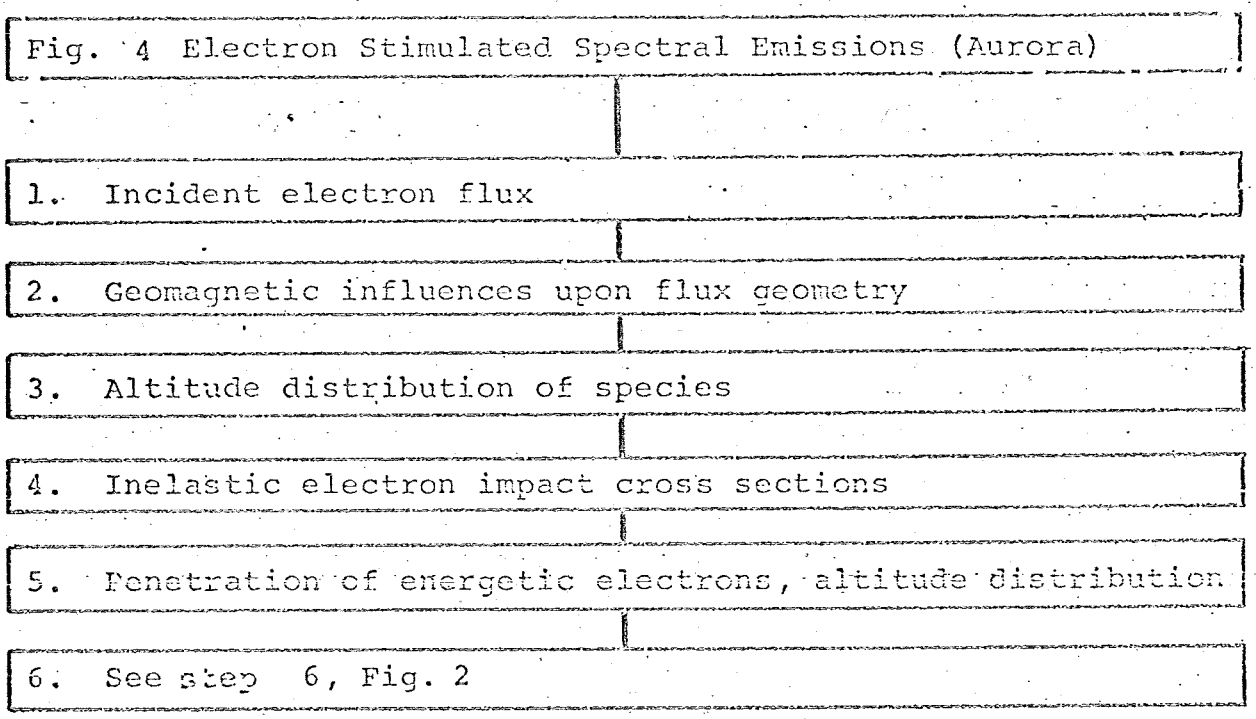
Fig. 4 Electron Stimulated Spectral Emissions (Aurora)
1. Incident electron flux
2. Geomagnetic influences upon flux geometry
3. Altitude distribution of species
4. Inelastic electron impact cross sections
5. Penetration of energetic electrons, altitude distribution
6. See step 6, Fig. 2

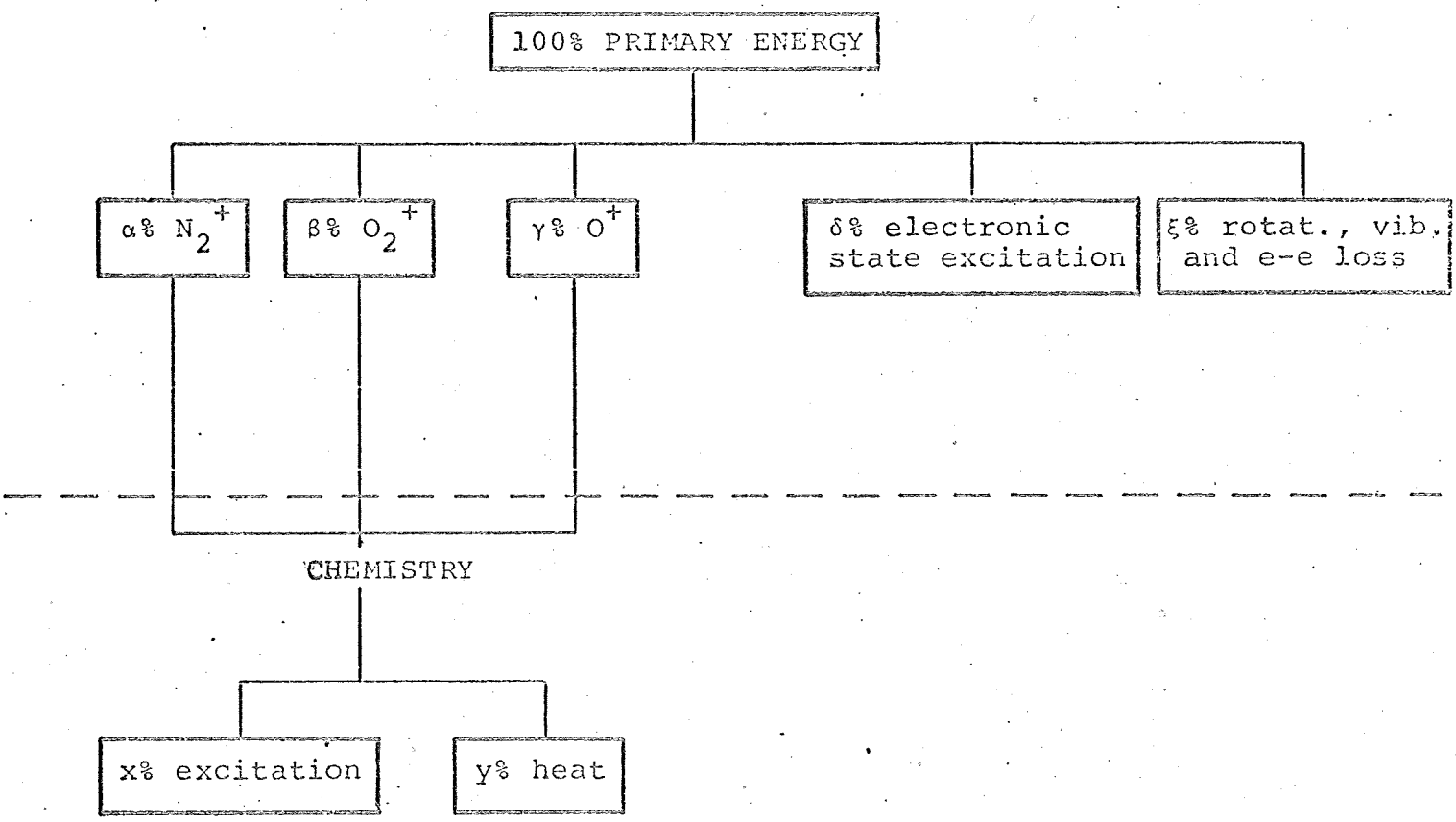
100% PRIMARY ENERGY
α% N_2^+
β% O_2^+
γ% O^+
δ% electronic state excitation
ξ% rotat., vib. and e-e loss
CHEMISTRY
x% excitation
y% heat

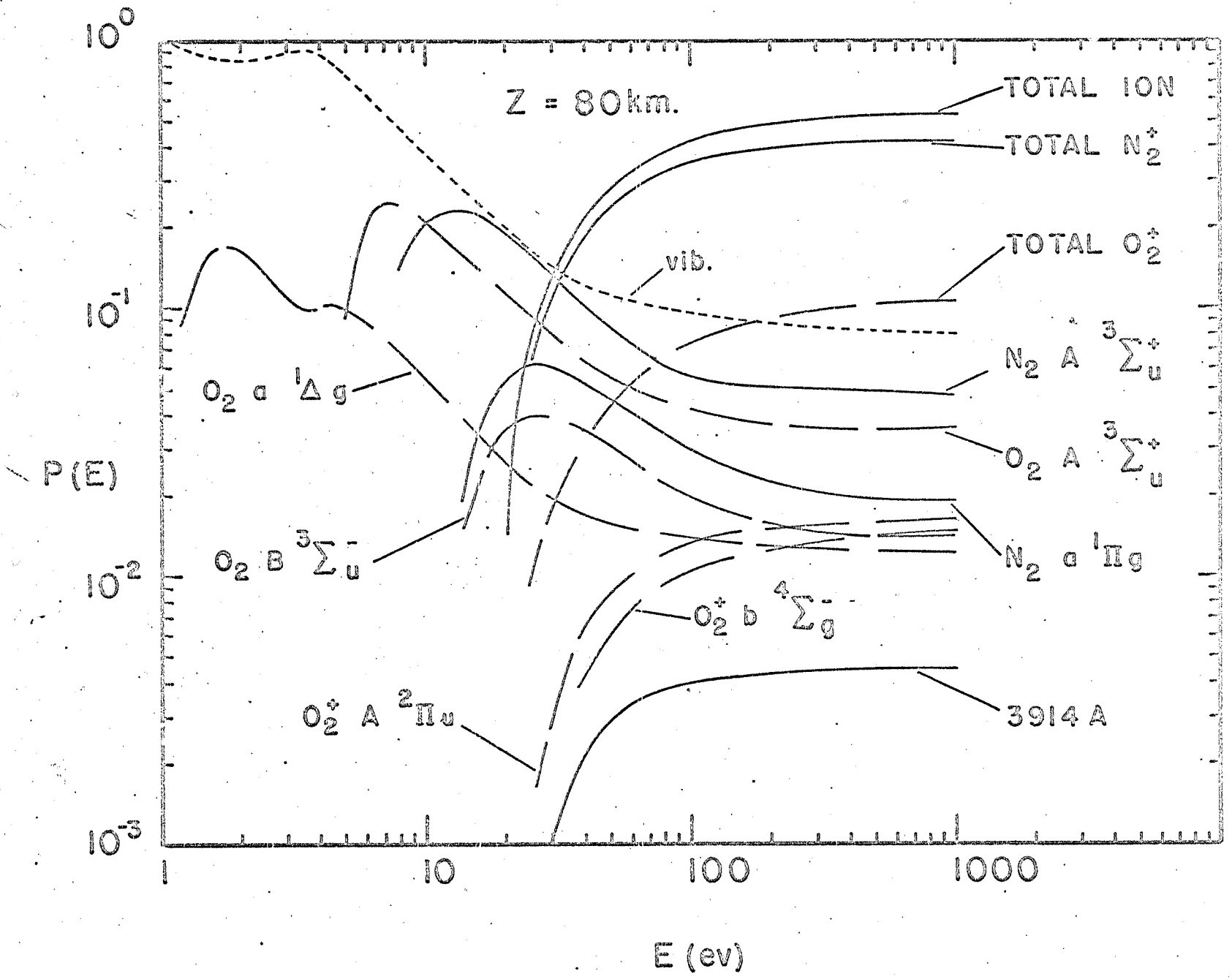
Z = 80km.
TOTAL ION
TOTAL N_2^+
TOTAL O_2^+
vib.
N_2 A $^3\Sigma_u^+$
O_2 A $^3\Sigma_u^+$
N_2 a $^1\Pi g$
O_2^+ b $^4\Sigma_g^-$
3914 A
O_2 a $^1\Delta g$
O_2 B $^3\Sigma_u^-$
O_2^+ A $^2\Pi u$
10^0
10^{-1}
10^{-2}
10^{-3}
P(E)
1
10
100
1000
E (ev)

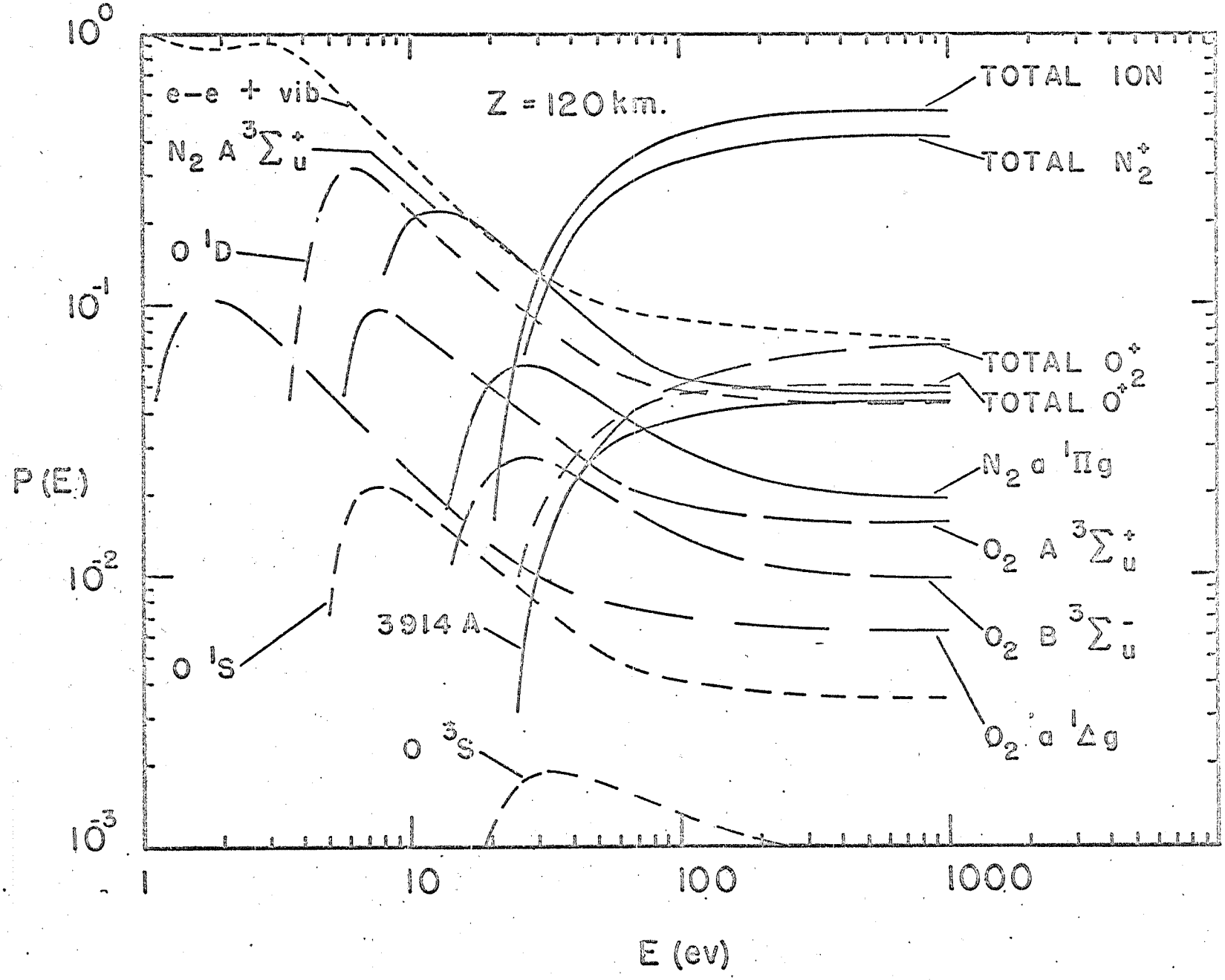
10^0
10^{-1}
10^{-2}
10^{-3}
P(E)
e–e + vib
Z = 120 km.
TOTAL ION
TOTAL N_2^+
N_2 A $^3\Sigma_u^+$
O ^{1}D
TOTAL O_2^+
TOTAL O^+
N_2 a $^1\Pi g$
O_2 A $^3\Sigma_u^+$
3914 A
O_2 B $^3\Sigma_u^-$
O ^{1}S
O_2 a $^1\Delta g$
O ^{3}S
1
10
100
1000
E (ev)

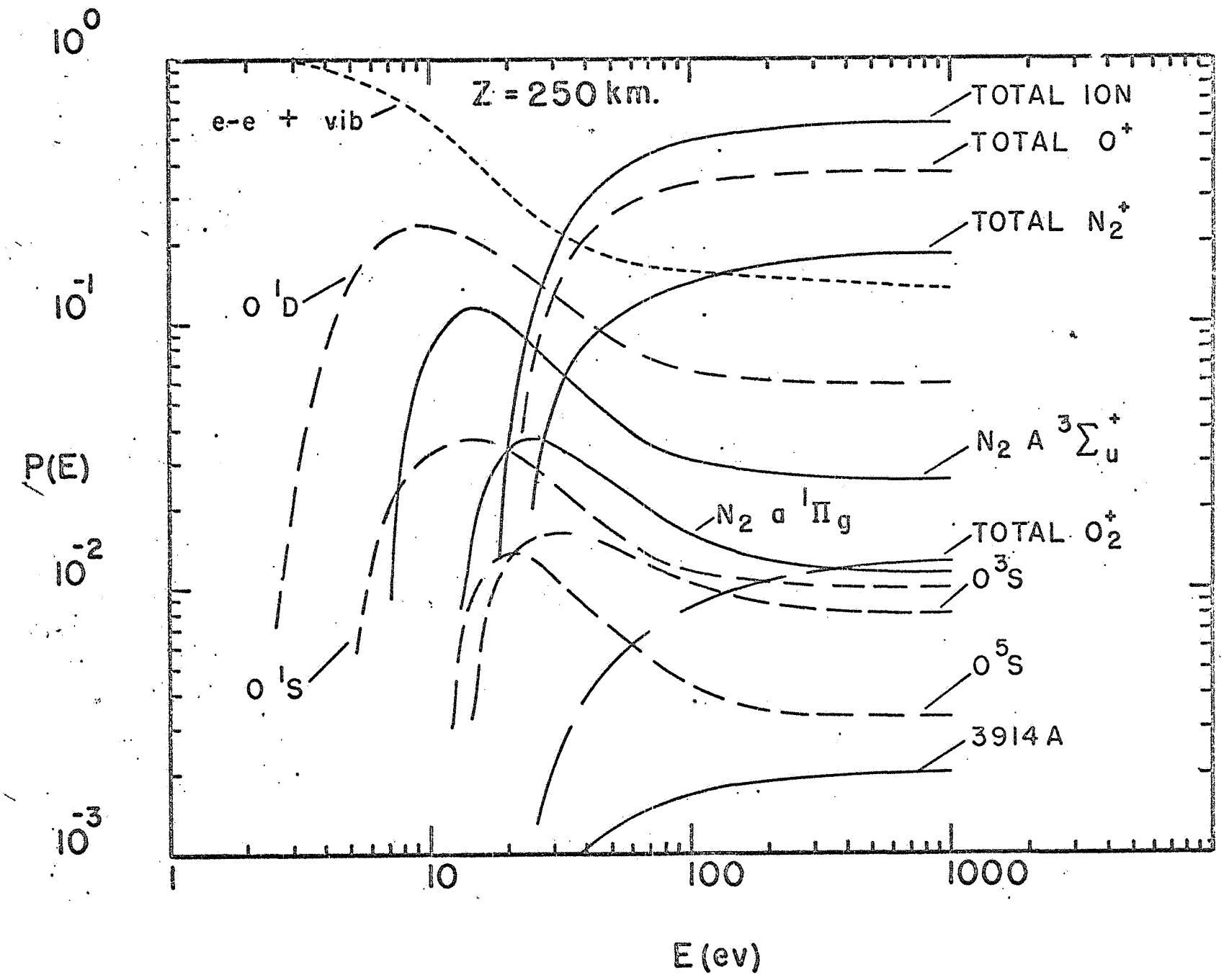
Z = 250 km.
e-e + vib
O 1D
O 1S
TOTAL ION
TOTAL O+
TOTAL N2+
N2 A 3Σu+
N2 a 1Πg
TOTAL O2+
O 3S
O 5S
3914 A
P(E)
E(ev)
10^0
10^-1
10^-2
10^-3
1
10
100
1000

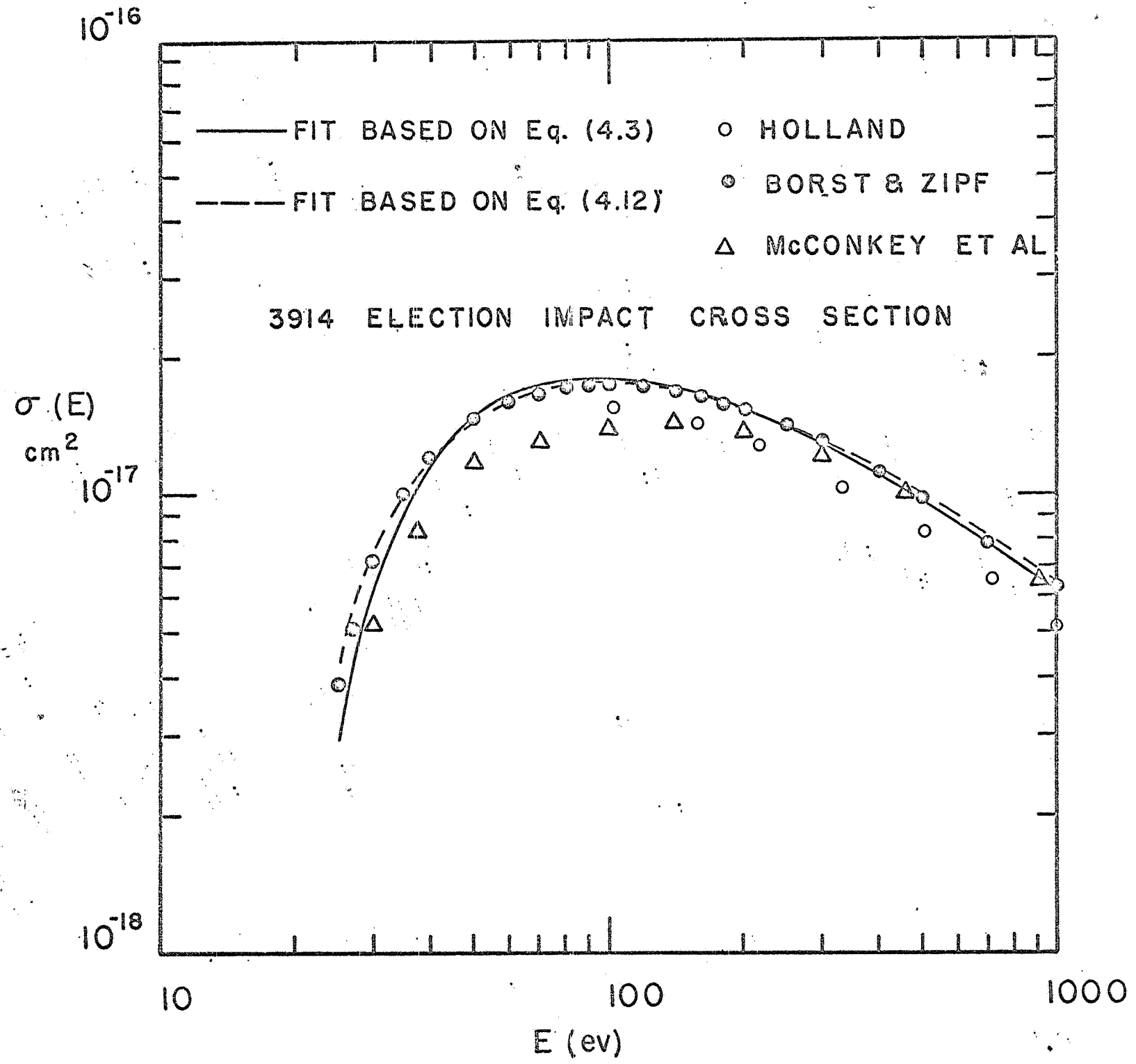
FIT BASED ON Eq. (4.3)
FIT BASED ON Eq. (4.12)
HOLLAND
BORST & ZIPF
McCONKEY ET AL
3914 ELECTION IMPACT CROSS SECTION
σ (E)
cm²
10⁻¹⁶
10⁻¹⁷
10⁻¹⁸
10
100
1000
E (ev)

Fig. 10

Reactions involved in a proton slowing down in N_2

Proton Induced

1.	$H^+ + N_2 \rightarrow H^+ + N_2^{(j)}$	excitation
2.	$H^+ + N_2 \rightarrow H^+ + N_2^+ + e$	ionization i
3.	$H^+ + N_2 \rightarrow H^+ + N_2^{++} + 2e$	double ionization di
4.	$H^+ + N_2 \rightarrow H^+ + N + N$	dissociation d
5.	$H^+ + N_2 \rightarrow H^{(n)} + N_2^{+(i)}$	capture c
6.	$H^+ + N_2 \rightarrow H^{(n)} + N_2^{++} + e$	ci
7.	$H^+ + N_2 \rightarrow H^{(n)} + N + N^+$	dissociative ionization
8.	$H^+ + N_2 \rightarrow H^- + N_2^{++}$	double capture

Incident Hydrogen Atoms

9.	$H^{(n)} + N_2 \rightarrow H^+ + N_2^j + e$	stripping s
10.	$H^{(n)} + N_2 \rightarrow H^+ + N_2^{+(i)} + 2e$	si
11.	$H^{(n)} + N_2 \rightarrow H^+ + N_2^{++} + 3e$	sdi
12.	$H^{(n)} + N_2 \rightarrow H^{(m)} + N_2^{(j)}$	transfer
13.	$H^{(n)} + N_2 \rightarrow H^{(m)} + N_2^{++} + 2e$	double ionization

Incident Negative Hydrogen Ions

14.	$H^- + N_2 \rightarrow H^{(n)} + N_2 + e$	stripping
15.	$H^- + N_2 \rightarrow H^+ + N_2 + 2e$	double stripping

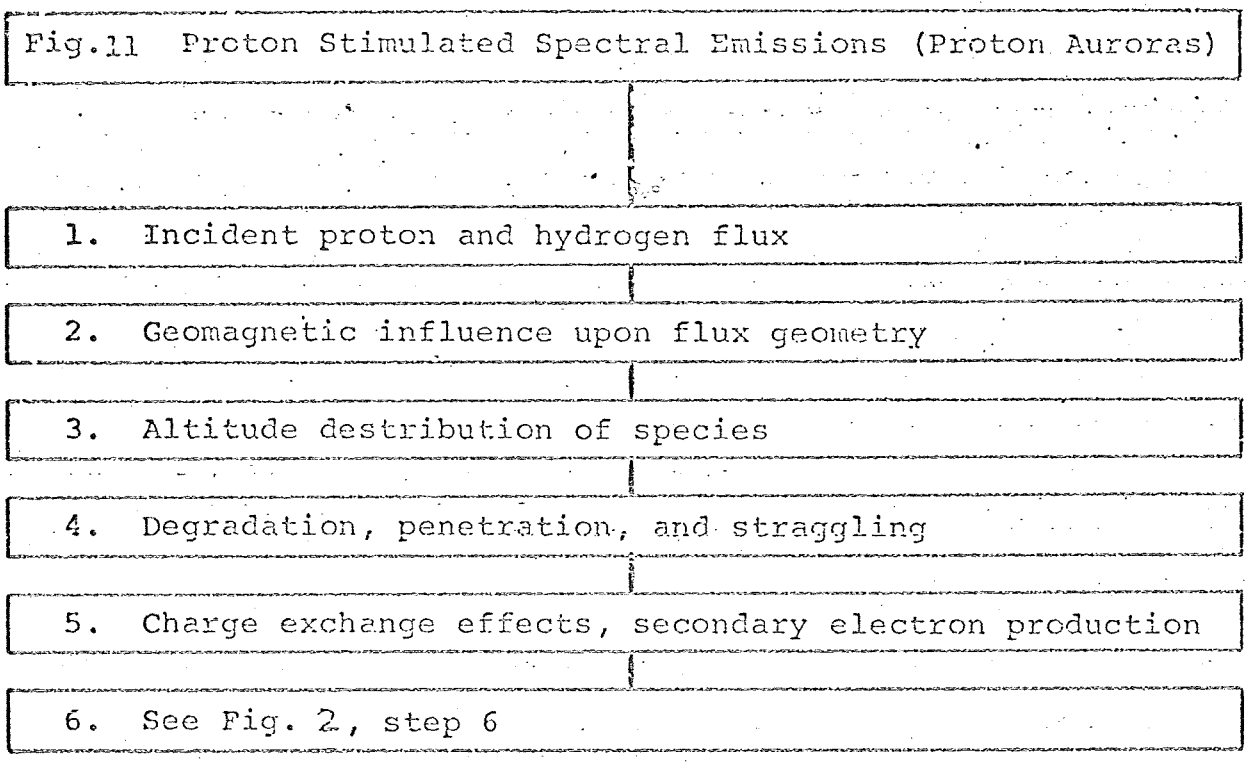
Fig.11 Proton Stimulated Spectral Emissions (Proton Auroras)
1. Incident proton and hydrogen flux
2. Geomagnetic influence upon flux geometry
3. Altitude destribution of species
4. Degradation, penetration, and straggling
5. Charge exchange effects, secondary electron production
6. See Fig. 2, step 6